

Active Polarization Control for Optical Fibres



Tan Jyh Harn
National University of Singapore
Department of Physics

A thesis submitted for the degree of
B.Sc. (Hons) in Physics

AY2017/2018

This thesis is dedicated to
my family and friends who have showed unwavering care and concern
to me and my fellow course mates who are completing this arduous
journey with me.

Acknowledgements

I would like to acknowledge the efforts of my project mentors, Yicheng and Hou Shun, for their help and advice, which without, this project would not have been possible. I sincerely thank them for their help despite their tight schedule and commitments to other ongoing projects. The polarisation compensation scheme, the core of this project, was of their work as well.

I would also like to acknowledge my fellow laboratory mates, Kenneth Ho, Aswin and Moe Thar for the valuable discussions which have gave me much needed advices in regards to the project. In particular, the coding advices by Moe Thar which have definitely help me save plenty of time.

I would also like to thank my supervisor, Professor Christian Kurtsiefer and Associate Professor Alexander Ling for giving me this opportunity to take up a final year project under the Centre for Quantum Technologies.

Last but not least, my course mates, who although are not doing the same project field with me, listened and gave advices to me when I face difficulties in the process of this project.

Abstract

Fibre-based Quantum Key Distribution (QKD) using polarization encoding requires a high fidelity of transmission. In this work, we use a set of Liquid Crystal Variable Retarders (LCVRs) to actively compensate for the polarization drift caused by a long fibre. We are able to maintain the transmitted horizontal polarization state at an error value of 0.01501 ± 0.01194 for a period of 6 hours using a simple gradient descent algorithm. This technique will be further explored in the future to prepare for a full scale implementation of a fibre QKD system.

Contents

| | |
|---|------------|
| Contents | i |
| List of Figures | iii |
| List of Tables | vi |
| 1 Introduction | 1 |
| 1.1 A Brief Introduction to QKDs | 1 |
| 1.2 Motivation | 2 |
| 2 Theory and Concepts | 5 |
| 2.1 The Polarisation of Light | 5 |
| 2.1.1 Stokes Parameters and Jones Vectors | 5 |
| 2.1.2 Mueller Calculus and Jones Matrix | 10 |
| 2.2 Optical Elements for Polarisation Control | 11 |
| 2.2.1 Wave Plates | 11 |
| 2.2.2 Liquid Crystal Variable Retarders | 13 |
| 2.3 Measuring Polarisation | 15 |
| 3 Experiment and Methodology | 17 |
| 3.1 Characterisation of Liquid Crystal Variable Retarders | 17 |
| 3.2 Polarisation Control Using LCVRs | 21 |
| 3.3 Setting Up The Polarimeter | 23 |
| 4 Results and Analysis | 28 |
| 4.1 Measuring Polarisation Drift | 28 |
| 4.2 Polarisation Compensation Results | 31 |
| 5 Conclusion and Further Discussions | 36 |

| | | |
|----------|--|-----------|
| A | Characterisation of Liquid Crystal Variable Retarders | 37 |
| B | Characterisation of Polarimeter | 41 |
| C | Constant Current Mode for Laser Driver | 44 |
| D | Polarisation Drift Compensation Code | 46 |
| | Bibliography | 51 |

List of Figures

| | | |
|------|--|----|
| 1.1 | A simplified diagram of the BBM92 protocol. | 1 |
| 2.1 | The commonly defined polarisation states of light as shown using a cartesian basis. Note that the \hat{k} component (out of page) is the direction of propagation. | 5 |
| 2.2 | The commonly polarised states represented on the Poincaré Sphere. Figure adapted from [1]. | 8 |
| 2.3 | Rotational effect on a linear input polarisation due to a half-wave plate. The rotation angle is twice the angle between the linear input polarisation axis and the optical axis of the half-wave plate. Figure from [2] | 12 |
| 2.4 | A quarter-wave plate transforms an linearly polarised input into a circular polarisation. Figure from [2] | 13 |
| 2.5 | Pictorial description of the construction of a typical liquid crystal cell. | 14 |
| 2.6 | Schematic of the optimal polarimeter and an example of four basis Stokes vector that maps out a tetrahedron. | 15 |
| 3.1 | Meadowlark Optic’s liquid crystal variable retarder | 17 |
| 3.2 | Schematic of the crossed polariser set-up. | 18 |
| 3.3 | Generated voltage waveform used to control the LCVRs. | 19 |
| 3.4 | Plot of mean raw voltage reading of photodetector vs LCVR voltage input for crossed polariser set-up in Figure 3.2. | 20 |
| 3.5 | Plot of LCVR retardance vs LCVR voltage input. | 21 |
| 3.6 | Poincaré sphere diagrams of LCVR coverage. | 22 |
| 3.7 | Simplified schematic of an array of four LCVRs. | 23 |
| 3.8 | Polarimeter. | 23 |
| 3.9 | Polarimeter characterisation set-up schematic. | 24 |
| 3.10 | Reconstruction of the Stokes vectors using the instrument matrix determined by the calibration states as shown on the Poincaré sphere. | 26 |

| | | |
|-----|--|----|
| 4.1 | Schematic of the toy model used to simulate polarisation drift. | 28 |
| 4.2 | Plot of Stokes parameters and degree of polarisation (DOP) of the laser output vs time to show fluctuation in polarisation across the 1km fibre spool. | 29 |
| 4.3 | Polarisation drift across the 1km fibre spool visualised on a Poincaré sphere. | 29 |
| 4.4 | Plot of Stokes parameters and DOP vs time in 1 hour to show fluctuation in polarisation across the 1km fibre spool. | 30 |
| 4.5 | Plot of Stokes parameters, DOP and Error vs time of polarisation across the 1km fibre spool but with active polarisation compensation code running. | 33 |
| 4.6 | Plot of Stokes parameters, DOP and Error vs time for the first 150s of polarisation output across the 1km fibre spool with active polarisation compensation code running. | 33 |
| 4.7 | Polarisation output across the 1km fibre spool with active polarisation compensation visualised on a Poincaré sphere. | 34 |
| 4.8 | Plot of LCVR voltage inputs vs time of polarisation output across the 1km fibre spool with active polarisation compensation code running. | 34 |
| 4.9 | Plot of LCVR voltage inputs for the first 150s of polarisation output across the 1km fibre spool with active polarisation compensation code running. | 35 |
| A.1 | Plot of mean raw voltage reading of photodetector vs LCVR voltage input for crossed polariser set-up in Figure 3.2 for the second LCVR. | 37 |
| A.2 | Plot of LCVR retardance vs LCVR voltage input for second LCVR. | 38 |
| A.3 | Plot of mean raw voltage reading of photodetector vs LCVR voltage input for crossed polariser set-up in Figure 3.2 for the third LCVR. | 38 |
| A.4 | Plot of LCVR retardance vs LCVR voltage input for third LCVR. | 39 |
| A.5 | Plot of mean raw voltage reading of photodetector for two separated data collection cycles. The voltage input is first increased from 0V to 10V then decreased from 10V to 0V. | 40 |
| A.6 | Plot of mean raw voltage reading of photodetector for two separated data collection cycles. The voltage input is first increased from 0V to 10V then decreased from 10V to 0V. | 40 |
| B.1 | Plot of mean normalised voltage readings of photodetectors in the polarimeter at each polarisation state input. | 41 |

| | | |
|-----|---|----|
| B.2 | Heat map of reconstructed Stokes vector shown in 3.10(ii). | 42 |
| B.3 | Plot of Degree of Polarisation (DOP) vs state input number | 43 |
| C.1 | Plot of Stokes parameters against time to show fluctuation in polarisation across the 1km fibre spool but at constant current mode. | 44 |
| C.2 | Polarisation drift across the 1km fibre spool visualised on a Poincaré sphere at constant current mode. | 45 |

List of Tables

| | | |
|-----|---|---|
| 2.1 | Stokes vector representation of the commonly defined polarisation states. | 8 |
|-----|---|---|

Chapter 1

Introduction

1.1 A Brief Introduction to QKDs

Quantum Key Distribution systems (QKDs) are protocols that can generate secure keys for cryptographic use by exploiting quantum mechanical properties. Such keys can be proven to be theoretically secure. Various protocols have been developed and each of these protocols utilises different quantum mechanical properties. QKDs generate these secure keys over public channels which can then be utilised by a classical private key cryptosystem [3]. As a result of the potentially tremendous benefits that QKDs can offer in cyber security, commercial QKDs has become an active research area in many large information technology companies such as Toshiba, Hewlett Packard, IBM and etc [4, 5, 6, 7].

We will briefly introduce QKDs. There are multiple protocols available [3, 8] but for convenience and relevance to this project, we will be discussing the Bennett-Brassard-Mermin 1992 (BBM92) protocol [9]

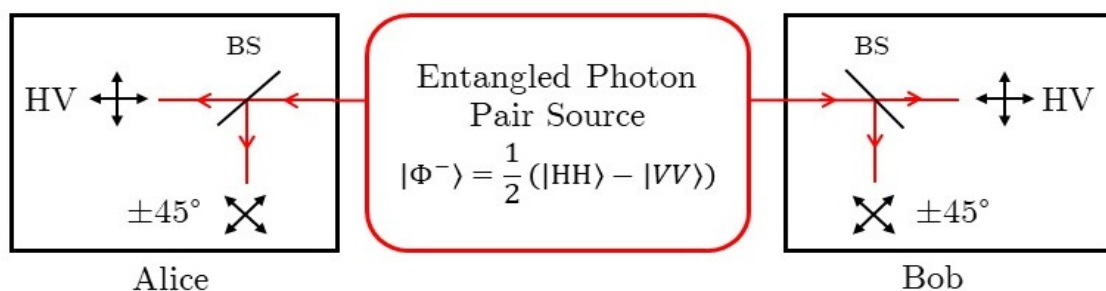


Figure 1.1: A simplified diagram of the BBM92 protocol.

Figure 1.1 shows a simplified method to establish a secure channel for communication between Alica and Bob. The photon pair source emits photon pairs with

the entangled state $|\Phi^-\rangle = \frac{1}{\sqrt{2}}(|HH\rangle - |VV\rangle)$. Both Alice and Bob have a 50:50 non-polarising beam splitter (BS) that will transmit or reflect the incoming photon into two different basis of polarisation measurement with equal probability. In this example, the two different measurement basis are Horizontal-Vertical (HV) basis and the diagonal linear $\pm 45^\circ$ basis.

After a sample of photons have been collected and measured, Alice and Bob will communicate via a classical channel to compare their sequence of measurement basis chosen. A process called sifting will be carried out where measurements done with different basis are discarded and those with the same basis will then be compared to check the measurement outcomes on both sides.

Suppose that there was no eavesdropper measuring the photon while it is being sent to Alice and Bob, the correlation of the sifted measurements will ideally be perfect and can be used to generate the private key shared between them. If an eavesdropper was present, then the correlation of the sifted measurements would be imperfect and Alice and Bob will be alerted to the presence of the eavesdropper. In this case, they can abandon this communication channel and try another one.

In a realistic context, the sifted measurement correlation will not be perfect due to environmental perturbations that adversely influence the correlation of the photon pair. The efficiency of the measurement devices and the reliability of the photon pair source are also factors affecting the outcome of a realistic correlation measurement. In practical applications, a threshold is set to determine if the channel is secured.

However, if the environmental perturbations (e.g. thermal fluctuations causing polarisation fluctuations) are significant, it could affect the usability of the protocol. In this project, we thus investigate a polarisation compensation scheme to counter the effects of polarisation drift to enhance the reliability of such QKDs that utilise polarisation states of photons for key generation.

1.2 Motivation

The polarisation state of photons can be readily controlled by conventional optical elements such as polarisers and waveplates, and plenty of polarimetry methods have been devised to measure the polarisation states [10, 11]. In QKDs protocols, photons are usually transmitted either through free space or optical fibres. Both transmission mediums have their pros and cons. However, for practical applications of QKDs, it is often easier to utilise existing optical fibres that connect end users of the internet service providers (ISPs), who will ultimately be the users of such commercial QKDs.

The end users of the ISPs will often be connected through optical fibre networks which can stretch over distances on the order of tens of kilometres. However, when transmitting photons over long optical fibres, the polarisation states of the transmitted photons fluctuates randomly over time. This is due to environmental temperature fluctuations, which causes thermal expansion and contraction, as well as mechanical oscillations which can alter the refractive index of the optical fibre at different segments [12]. As a result, the fidelity of the photon polarisation state being transmitted is severely affected and poses an issue to the feasibility of QKDs over long distances.

This issue has been addressed by multiple experiments using different methodologies and on different key bits basis such as photon phase [12, 13, 14]. These methodologies in general are called compensation schemes which rectifies the error or fluctuation due to the environment in which the QKDs are implemented in. While these experiments have proven successful, they usually involved more complex set-up such as Dense Wavelength Division Multiplexing (DWDM) systems [12] or the use of multiple reference pulses [13, 14] for feedback in the compensation scheme.

There also exist polarisation-maintaining optical fibres that can prevent polarisation drifts. However, it is not easy to implement as it requires the polarisation input to be directed in the birefringent axes. This means that the fibre may need to be readjusted should the polarisation input change. Furthermore, power loss through polarisation-maintaining optical fibres is usually higher than standard optical fibres which can be a problem for long distance usage, such as implementing it for city wide telecommunication purposes [15].

In this project, a simpler and more direct polarisation compensation scheme is tested to minimise polarisation fluctuation about some arbitrary defined polarisation state. The main optical component responsible for compensating the polarisation drift is the liquid crystal variable retarder (LCVR). An array of LCVRs is lined up, each with its optical axis tilted at some angle, to provide enough degree of freedom to modify any polarisation input into any desired output. Each of the individual LCVR is connected to a function generator to control its retardance.

By using an simple correction algorithm to control the LCVRs, along with the fast response time of the LCVR ($\sim 10\text{ms}$), we find that the LCVRs can be effective in compensating polarisation drifts. Such compensation scheme can prove useful to various QKDs utilising polarisation states as basis for key generation, as long the correction algorithm is modified accordingly to fit the protocol.

In this report, we first explore the relevant mathematical preliminaries and concepts about the polarisation of light in Chapter 2. These will allow us to better under-

stand the workings of LCVRs and other optical components of the set-up. In Chapter 3, we will explain the technical process of setting up the polarisation compensation set-up. Following that, in Chapter 4, we discuss further in detail the methodology of measurements taken. The results and analysis of the final compensation test is then discussed. Finally, we conclude the report in Chapter 5.

Chapter 2

Theory and Concepts

2.1 The Polarisation of Light

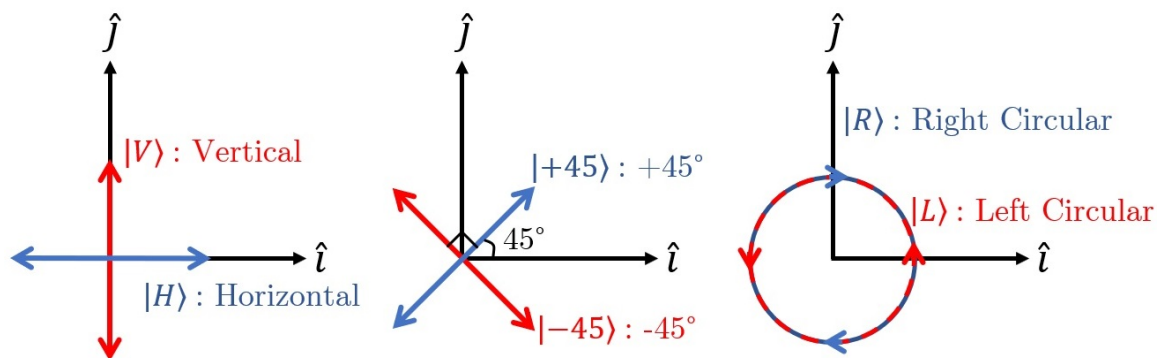


Figure 2.1: The commonly defined polarisation states of light as shown using a cartesian basis. Note that the \hat{k} component (out of page) is the direction of propagation.

We understand that light can be described as transverse electromagnetic waves. For an electromagnetic wave, the electric field component, \vec{E} , and propagation vector, \vec{k} , is used to define the polarisation state of light and it lies in the plane-of-vibration of the electric field.

The behaviour and polarisation of light can be described by the wave equations. In this section, we will instead present some mathematical constructs that describe the polarisation of light in a more convenient manner without the need of the more rigorous wave equation treatment.

2.1.1 Stokes Parameters and Jones Vectors

G. G. Stokes formulated the Stokes parameters in 1852 to describe the polarisation of light with observables of the electromagnetic wave, specifically intensity [16]. There

are 4 parameters and as each parameter are functions of observables, they can be measured and obtained directly. The parameters can be obtained as such:

1. The beam of light under investigation is sampled with 4 different filters. Each of these filters, when exposed to incident unpolarised light, will only transmit half of the incident intensity.
2. The first filter is isotropic and allows all polarisation states to pass through equally, the intensity reading yield after this filter is I_0 .
3. The second filter only transmits horizontally polarised light which yields another intensity reading, I_1 .
4. The third filter only transmits $+45^\circ$ polarised light which yields the third intensity reading, I_2 .
5. The fourth filter only transmits right circularly polarised light, which yields the third intensity reading, I_3 .

With these four intensity readings, we can construct the four Stokes parameters as such

$$\begin{aligned}
 S_0 &= 2I_0 \\
 S_1 &= 2I_1 - 2I_0 \\
 S_2 &= 2I_2 - 2I_0 \\
 S_3 &= 2I_3 - 2I_0
 \end{aligned}
 \tag{2.1}$$

From the 4 relations stated in Equation 2.1, we can clearly see that S_0 represents the total intensity of the light beam under investigation or the incident irradiance. S_1 represents the degree of horizontal polarisation and it's orthogonal basis of vertical polarisation. S_2 represents the degree of $+45^\circ$ polarisation and its orthogonal basis of -45° polarisation. Finally, S_3 represents the degree of right circularly polarisation and it's orthogonal basis of left circularly polarisation.

Here we state the vector components of a quasi-monochromatic light [16] in an attempt to relate the wave treatment to the Stokes parameters we have defined in Equation 2.1.

$$\begin{aligned}
 \vec{E}_x(t) &= E_{0x}(t) \cos[(kz - \omega t) + \epsilon_x(t)]\hat{\mathbf{i}} \\
 \vec{E}_y(t) &= E_{0y}(t) \cos[(kz - \omega t) + \epsilon_y(t)]\hat{\mathbf{j}} \\
 \vec{E}(t) &= \vec{E}_x(t) + \vec{E}_y(t)
 \end{aligned}
 \tag{2.2}$$

Where the electric field components are simply expressed in the typical $\hat{\mathbf{i}}$ (horizontal) and $\hat{\mathbf{j}}$ (vertical) basis from Cartesian coordinates. In this case, the direction of propagation is in the $\hat{\mathbf{k}}$ direction. The relative phase difference between the two components, $\epsilon = \epsilon_y - \epsilon_x$. Under the assumption that the incident light is perfectly monochromatic, we use the understanding in Equation 2.1 to recast the Stokes parameter using Equation 2.2 such that

$$\begin{aligned} S_0 &= \langle E_{0x}^2 \rangle_T + \langle E_{0y}^2 \rangle_T \\ S_1 &= \langle E_{0x}^2 \rangle_T - \langle E_{0y}^2 \rangle_T \\ S_2 &= \langle 2E_{0x}E_{0y} \cos(\epsilon) \rangle_T \\ S_3 &= \langle 2E_{0x}E_{0y} \sin(\epsilon) \rangle_T \end{aligned} \quad (2.3)$$

Where the subscript T denotes time average.

If the incident light is unpolarised, then we can see that $\langle E_{0x}^2 \rangle_T = \langle E_{0y}^2 \rangle_T$ but $S_1 = S_2 = S_3 = 0$. It can also be shown that for a fully polarised light, the following relation must be obeyed

$$S_0^2 = S_1^2 + S_2^2 + S_3^2 \quad (2.4)$$

Since the Stokes parameters are intensity readings, we can normalise them to the total intensity, S_0 for simplicity and by writing the normalised Stokes parameters as the elements of a 4 component vector, we form the normalised Stokes vector i.e. $(S_0, S_1, S_2, S_3) \longrightarrow (1, S_1/S_0, S_2/S_0, S_3/S_0)$. Along with Equation 2.4, this leads to the quantity, degree of polarisation,

$$V = \frac{\sqrt{S_1^2 + S_2^2 + S_3^2}}{S_0} \quad (2.5)$$

We can clearly see if the incident light is unpolarised, then $V = 0$. If the light is polarised, Equation 2.4 shows that $V = 1$. Any value in between 0 to 1 is considered partially polarised.

By considering the common polarisation states, namely, horizontal, vertical, $+45^\circ$, -45° , left circular and right circular, we can summarise the results in terms of the normalised Stokes vectors as such

| Polarisation States | Stokes vector $(1, S_1/S_0, S_2/S_0, S_3/S_0)$ |
|---------------------|--|
| Horizontal | $(1, 1, 0, 0)$ |
| Vertical | $(1, -1, 0, 0)$ |
| +45° | $(1, 0, 1, 0)$ |
| -45° | $(1, 0, -1, 0)$ |
| Right circular | $(1, 0, 0, 1)$ |
| Left circular | $(1, 0, 0, -1)$ |

Table 2.1: Stokes vector representation of the commonly defined polarisation states.

From Table 2.1, we see that the second component (S_1/S_0) represents the degree of linear polarisation in the horizontal-vertical basis, with $(S_1/S_0) = 1$ for horizontal polarisation and $(S_1/S_0) = -1$ for vertical polarisation. The same goes for the other components as well. At the same time, we see the convenience of using the Stokes vector to describe the polarisation state of light.

We previously normalised the Stokes parameters to the total intensity for a good reason. The normalised Stokes parameters S_1/S_0 , S_2/S_0 and S_3/S_0 are used as Cartesian coordinates for the Poincaré sphere.

The Poincaré sphere was introduced by Henri Poincaré in 1892 [10]. It is a useful graphical visualisation of the polarisation states of light. Referring back to Equations 2.4 and 2.5, if one maps out all the polarised states using the normalised Stokes parameters as Cartesian coordinates, a unit sphere is obtained. Any partially polarised states will be a vector lying within the sphere and the unpolarised state will be a point at the centre of the sphere. It thus has the ability to represent all the possible polarisation states of light.

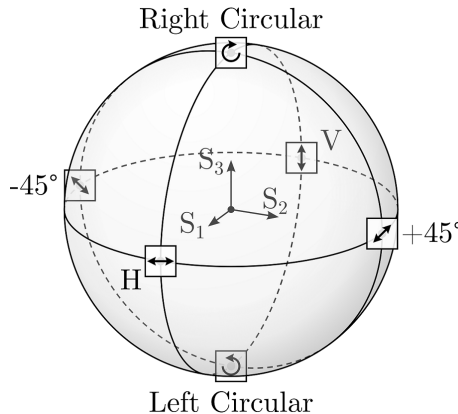


Figure 2.2: The commonly polarised states represented on the Poincaré Sphere. Figure adapted from [1].

We see from Figure 2.2 that the linear polarisations fall on the equator of the sphere while the circular polarisation falls on the poles. Any other polarisation on the surface represents elliptical polarisation states. This tool will later be useful in visualising the polarisation drift of light through long optical fibres.

At the same time, we also introduce the Jones vector, which is another representation of light. However, this representation is only applicable to fully polarised light. It is a vertical two-component vector that is expressed in terms of the electric field vector components as described in Equation 2.2.

However, instead of writing out in full, we simplify in complex exponential form as shown below

$$\tilde{\mathbf{E}} = \begin{pmatrix} E_{0x}e^{i\phi_x} \\ E_{0y}e^{i\phi_y} \end{pmatrix} \quad (2.6)$$

Where ϕ_x and ϕ_y are the appropriate phases and, E_{0x} and E_{0y} are the amplitude of the x and y component respectively. We see that only the amplitude of each components remains as the temporal components are now encoded in the phase factors.

Suppose the light is horizontally and vertically polarised. We then obtain respectively

$$\tilde{\mathbf{E}}_{\mathbf{H}} = \begin{pmatrix} E_{0x}e^{i\phi_x} \\ 0 \end{pmatrix} \text{ and } \tilde{\mathbf{E}}_{\mathbf{V}} = \begin{pmatrix} 0 \\ E_{0y}e^{i\phi_y} \end{pmatrix} \quad (2.7)$$

Suppose $\phi_x = \phi_y$ and $E_{0x} = E_{0y}$, we will then get the representation for a $+45^\circ$ polarised light

$$\tilde{\mathbf{E}}_{+45^\circ} = \tilde{\mathbf{E}}_{\mathbf{H}} + \tilde{\mathbf{E}}_{\mathbf{V}} = E_{0x} \begin{pmatrix} 1 \\ 1 \end{pmatrix} \quad (2.8)$$

Suppose the y-component leads the x-component by $\frac{\pi}{2}$ phase and that $E_{0x} = E_{0y}$, we will then get the representation for a right circularly polarised light

$$\tilde{\mathbf{E}}_{\mathbf{R}} = \begin{pmatrix} E_{0x}e^{i\phi_x} \\ E_{0x}e^{i(\phi_x - \frac{\pi}{2})} \end{pmatrix} \quad (2.9)$$

Which is still rather complex. However, if we were to normalised the amplitude to 1 (i.e. $|\tilde{\mathbf{E}}|^2 = 1$) and take away common factors on both components, we can see that the Jones vectors listed in Equations 2.7, 2.8 and 2.9 can be reduced to

$$\tilde{\mathbf{E}}_{\mathbf{H}} = \begin{pmatrix} 1 \\ 0 \end{pmatrix}, \tilde{\mathbf{E}}_{\mathbf{V}} = \begin{pmatrix} 0 \\ 1 \end{pmatrix}, \tilde{\mathbf{E}}_{+45^\circ} = \frac{1}{\sqrt{2}} \begin{pmatrix} 1 \\ 1 \end{pmatrix} \text{ and } \tilde{\mathbf{E}}_{\mathbf{R}} = \frac{1}{\sqrt{2}} \begin{pmatrix} 1 \\ -i \end{pmatrix} \quad (2.10)$$

along with the remaining common polarisation states (-45° and left circular)

$$\tilde{\mathbf{E}}_{-45^\circ} = \frac{1}{\sqrt{2}} \begin{pmatrix} 1 \\ -1 \end{pmatrix} \text{ and } \tilde{\mathbf{E}}_{\mathbf{L}} = \frac{1}{\sqrt{2}} \begin{pmatrix} 1 \\ i \end{pmatrix} \quad (2.11)$$

Comparing to the Stokes vectors, the Jones vectors appears to be more straightforward and can be useful for the analysis of the polarisation of light. For example, to find the effects of combining two coherent polarised light wave such as horizontally and vertically polarised light, a linear sum will do the trick

$$\tilde{\mathbf{E}}_{\mathbf{H}} + \tilde{\mathbf{E}}_{\mathbf{V}} = \begin{pmatrix} 1 \\ 1 \end{pmatrix} = \sqrt{2}\tilde{\mathbf{E}}_{+45^\circ} \quad (2.12)$$

which is a $+45^\circ$ polarised light with twice the intensity.

It is also able to encode phase information directly unlike Stokes vectors where additional calculation is needed (in the case of fully polarised light). However, the only disadvantage of Jones vectors is that is can only be used for fully polarised light.

It is shown in Equation 2.3 how to convert between Jones and Stokes vectors.

2.1.2 Mueller Calculus and Jones Matrix

Having understood that the polarisation state of light can be expressed in terms of the Stokes and Jones vector, we now proceed to review the mathematical representation of optical devices that can interact or manipulate the polarisation state of light.

Vectors can be transformed through matrix multiplication with a transformation matrix. This is the same for both Stokes and Jones vectors. This transformation process represents the manipulation of the polarisation state through the use of optical elements such as polarisers and retarders. Hence, such optical elements can be represented by a 4×4 matrix in the case of Stokes vectors and 2×2 matrix in the case of Jones vectors.

The 4×4 matrices are called Mueller matrices and are developed by Hans Mueller in 1943 [16] while the 2×2 matrices are the Jones matrices.

As an example, we consider a simple case of a horizontally polarised light transmitting through a $+45^\circ$ transmission linear polariser, the process can be described as such

$$\frac{1}{2} \begin{pmatrix} 1 & 0 & 1 & 0 \\ 0 & 0 & 0 & 0 \\ 1 & 0 & 1 & 0 \\ 0 & 0 & 0 & 0 \end{pmatrix} \begin{pmatrix} 1 \\ 1 \\ 0 \\ 0 \end{pmatrix} = \frac{1}{2} \begin{pmatrix} 1 \\ 0 \\ 1 \\ 0 \end{pmatrix} \quad (2.13)$$

for the case of Mueller matrix and for the case of Jones representation, it will be

$$\frac{1}{2} \begin{pmatrix} 1 & 1 \\ 1 & 1 \end{pmatrix} \begin{pmatrix} 1 \\ 1 \end{pmatrix} = \frac{1}{2} \begin{pmatrix} 1 \\ 1 \end{pmatrix} \quad (2.14)$$

The above equations basically show the output is a $+45^\circ$ polarised light with half the intensity relative to the input intensity.

We see that both the Mueller and Jones matrices are very convenient methods to represent optical elements interacting with the polarisation state of light. We will further introduce more optical elements and their representing matrices along the report.

2.2 Optical Elements for Polarisation Control

In optical experiments, wave plates and linear polarisers are commonly used optical elements. In general, wave plates are retarders that shifts the phase of one electric field component relative to the corresponding orthogonal component, resulting in a change in polarisation state. Polarisers on the other hand allows the transmission of certain polarisation states while filtering or attenuating others.

2.2.1 Wave Plates

The relative retardation of the orthogonal electric field components is possible because of a material property known as birefringence [16] where the refractive index varies with the propagation axis. The axis which slows down the propagation of the electric field component more relative to it's orthogonal axis is known as the slow axis. The orthogonal axis is known as the fast axis.

The retardation of the orthogonal components by the wave plate is dependent on the wavelength of the incident light (assuming a coherent light source), the physical dimension and refractive index of the wave plate. These will determine the optical path length experienced by different polarisation components of the incident light and hence its relative retardance. The overall relation can be summarised as

$$\Delta\phi = \frac{2\pi d(n_1 - n_2)}{\lambda} \quad (2.15)$$

Where $\Delta\phi$ is the overall phase shift, d is the thickness of the wave plate, n_1 is the refractive index along the slow axis, n_2 is the refractive index along the fast axis and λ is the wavelength of the incident light.

Without jumping into excessive mathematical derivations, we directly introduce two commonly used fixed retardance wave plates, namely the half-wave plate and quarter-wave plate.

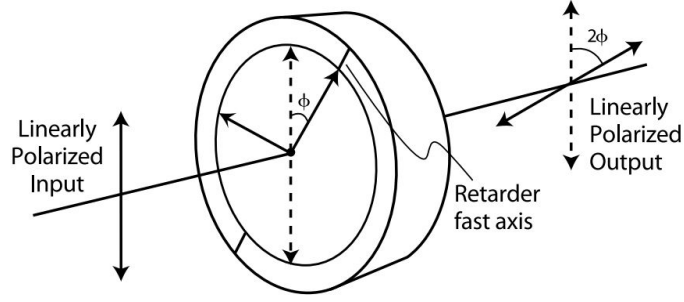


Figure 2.3: Rotational effect on a linear input polarisation due to a half-wave plate. The rotation angle is twice the angle between the linear input polarisation axis and the optical axis of the half-wave plate. Figure from [2]

The half-wave plate introduces a relative phase difference of π radians between the slow axis and fast axis, or in terms of wavelength, a shift by $\frac{\lambda}{2}$ between the orthogonal electric field components. It is commonly used to rotate the angle of the electric field in the transverse plane of the linearly polarised light with respect to angle of the fast axis of the half-wave plate. As for circular polarisation, it transforms it to the orthogonal polarisation, i.e. right circular polarisation to left circular polarisation or vice versa.

If we consider a situation where a $+45^\circ$ polarised light is transmitted across the half-wave plate aforementioned, the result will be as such

$$\begin{pmatrix} 1 & 0 & 0 & 0 \\ 0 & 1 & 0 & 0 \\ 0 & 0 & -1 & 0 \\ 0 & 0 & 0 & -1 \end{pmatrix} \begin{pmatrix} 1 \\ 0 \\ 1 \\ 0 \end{pmatrix} = \begin{pmatrix} 1 \\ 0 \\ -1 \\ 0 \end{pmatrix} \quad \text{and} \quad i \begin{pmatrix} 1 & 0 \\ 0 & -1 \end{pmatrix} \frac{1}{\sqrt{2}} \begin{pmatrix} 1 \\ 1 \end{pmatrix} = \frac{i}{\sqrt{2}} \begin{pmatrix} 1 \\ -1 \end{pmatrix}$$

The emerging light will now be rotated by $\frac{\pi}{2}$ radians and it becomes a -45° polarised light beam. The complex coefficient in the Jones representation can be neglected since there is no relative phase shift between the two components.

The quarter-wave plate introduces a relative phase difference of $\frac{\pi}{2}$ radians and in terms of wavelength, a shift of $\frac{\lambda}{4}$. It is commonly used to convert linear polarised light to circularly polarised light and vice-versa.

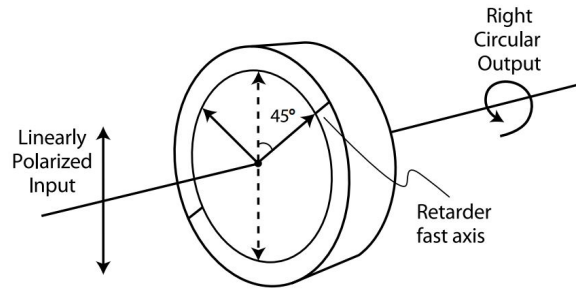


Figure 2.4: A quarter-wave plate transforms an linearly polarised input into a circular polarisation. Figure from [2]

Again, for demonstration of the effects of the quarter-wave plate, we consider the case of a $+45^\circ$ polarised light being transmitted across the quarter-wave plate with its fast-axis vertical

$$\begin{pmatrix} 1 & 0 & 0 & 0 \\ 0 & 1 & 0 & 0 \\ 0 & 0 & 0 & -1 \\ 0 & 0 & 1 & 0 \end{pmatrix} \begin{pmatrix} 1 \\ 0 \\ 1 \\ 0 \end{pmatrix} = \begin{pmatrix} 1 \\ 0 \\ 0 \\ 1 \end{pmatrix} \quad \text{and} \quad e^{i\frac{\pi}{4}} \begin{pmatrix} 1 & 0 \\ 0 & -i \end{pmatrix} \frac{1}{\sqrt{2}} \begin{pmatrix} 1 \\ 1 \end{pmatrix} = e^{i\frac{\pi}{4}} \begin{pmatrix} 1 \\ -i \end{pmatrix}$$

The emerging now a right circularly polarised light, an effect that arises when the orthogonal electric field components becomes $\frac{\pi}{2}$ out of phase relative to each other. Again, in the case of the Jones representation the $e^{i\frac{\pi}{4}}$ factor can be neglected given that there is no relative phase shift between both orthogonal electric field components after the transformation.

2.2.2 Liquid Crystal Variable Retarders

Besides wave plates with fixed retardance, there are also optical devices that can have varying retardance. A commonly used variable retarder known as the liquid crystal variable retarder (LCVR) is one example and is the main optical component used in this project.

A liquid crystal refers to a phase of matter that possess physical properties of both solids and liquids [16]. Typically, liquid crystals consist of elongated molecules and how these molecules align with respect to each other determine the type of liquid crystal.

The nematic liquid crystals are of relevance in this project. The nematic liquid crystals are made up of molecules that tend to align together in one general direction known as the *director*. Due to its elongated structure and orientation, the liquid crystals acts together as an anisotropic dielectric [16]. The long axis of the molecules

determines the slow axis or the optical axis of the liquid crystal which is responsible for the birefringent property of the liquid crystals.

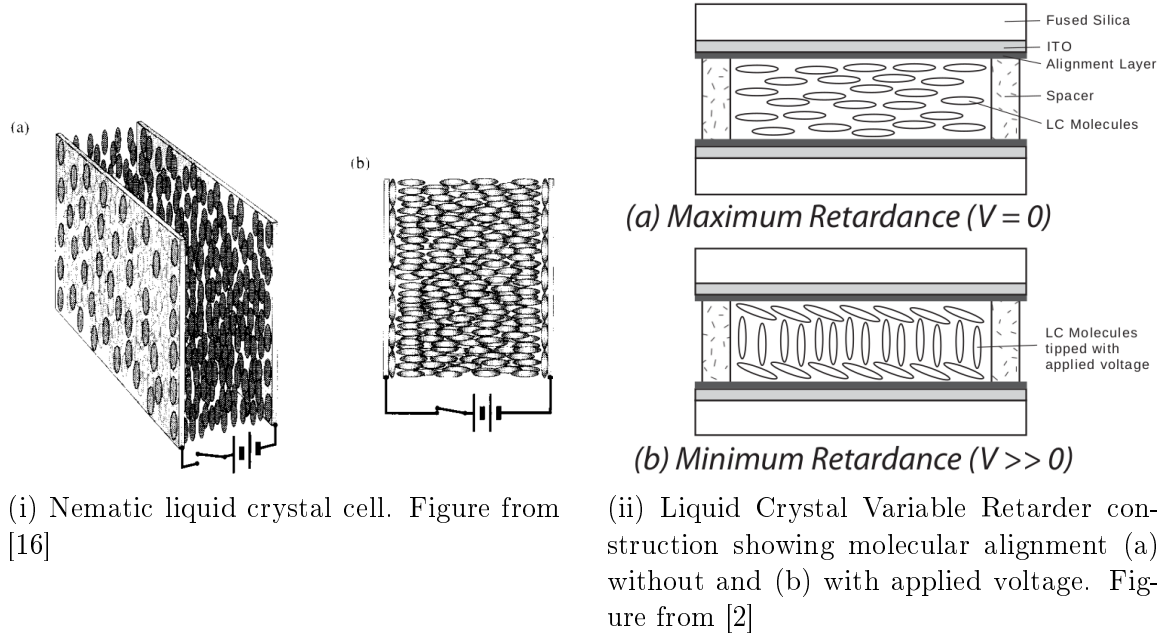


Figure 2.5: Pictorial description of the construction of a typical liquid crystal cell.

Making use of this property of nematic liquid crystals, variable retarders can be constructed, like the one shown in Figure 2.5(i). A layer of the liquid crystal is coated on a transparent electrically conducting film present on the inward facing sides of the parallel planar glass, usually indium tin oxide (ITO). These coatings on both glass pieces will form the alignment layer in which the rest of the liquid crystal in between the two films will align to, as shown in Figure 2.5(ii).

When an electric field is applied across the nematic cell, an electric dipole moment is induced among the liquid crystal molecules, causing a torque that rotates the crystal to align with the electric field. The stronger the electric field, the more the molecule long axis is inclined to the direction of the electric field. As a result, the birefringence is varied continuously, from high retardance to low retardance, forming a variable retarder.

The variable retarder can also be represented as a Mueller matrix [10] as well

$$\begin{pmatrix} 1 & 0 & 0 & 0 \\ 0 & \cos^2(2\theta) + \cos(\phi) \sin^2(2\theta) & [1 - \cos(\phi)] \sin(2\theta) \cos(2\theta) & -\sin(\phi) \sin(2\theta) \\ 0 & [1 - \cos(\phi)] \sin(2\theta) \cos(2\theta) & \sin^2(2\theta) + \cos(\phi) \cos^2(2\theta) & \sin(\phi) \cos(2\theta) \\ 0 & \sin(\phi) \sin(2\theta) & -\sin(\phi) \cos(2\theta) & \cos(\phi) \end{pmatrix}$$

and also in the Jones matrix representation [10]

$$\begin{pmatrix} \cos\left(\frac{\phi}{2}\right) + i \sin\left(\frac{\phi}{2}\right) \cos(2\theta) & i \sin\left(\frac{\phi}{2}\right) \sin(2\theta) \\ i \sin\left(\frac{\phi}{2}\right) \sin(2\theta) & \cos\left(\frac{\phi}{2}\right) - i \sin\left(\frac{\phi}{2}\right) \cos(2\theta) \end{pmatrix}$$

Where θ is the angle of the fast optical axis from the horizontal axis and ϕ is the retardance induced.

2.3 Measuring Polarisation

Aside from understanding the mathematical description of the polarisation states of light, we also need to measure it as well since a compensation scheme requires constant monitoring of the polarisation. Devices that measure the polarisation state of light are known as polarimeters and the method of measurement is also known as polarimetry. Plenty of polarimetry methods are available [10] but for simplicity, a minimal scheme of polarisation measurement is used in this project.

Our minimal polarimetry method follows closely to [11] and is a form of division-of-amplitude polarimeter. This method is considered both minimal (least measurement needed) and optimal (least uncertainty in measurement and determines all input polarisation states equally well).

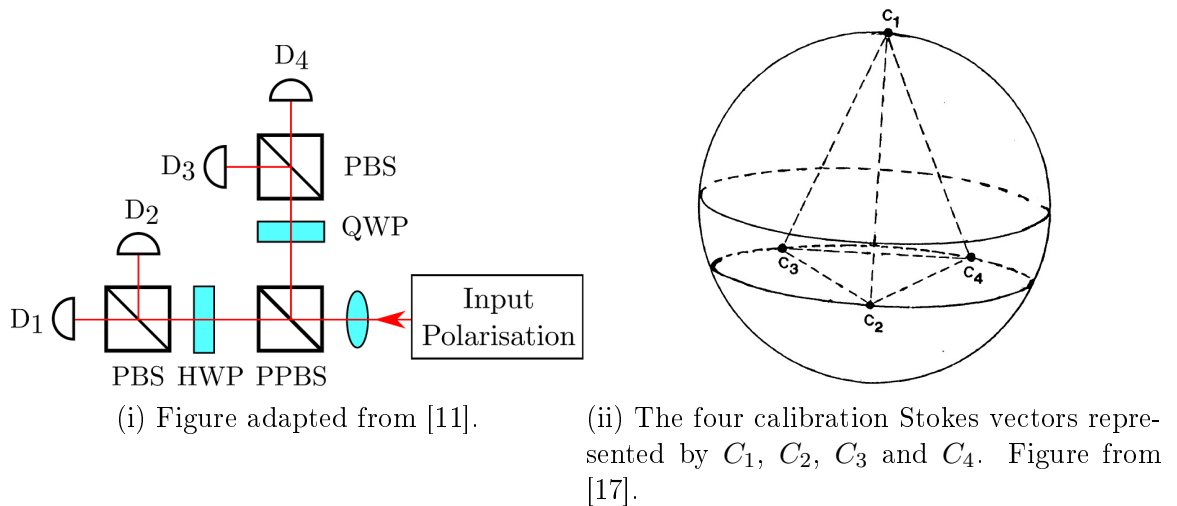


Figure 2.6: Schematic of the optimal polarimeter and an example of four basis Stokes vector that maps out a tetrahedron.

This polarimeter works in the following way. The input light is partially split into two arms at the partially polarising beam splitter (PPBS) with a transmit-reflect splitting ratio of 79:21 for horizontal polarisation and vice-versa for vertical polarisation

The transmitted and reflected arms transfer different proportions of intensities of the orthogonal electric field components. The two daughter beams are then each further split into 2 beams by their respective polarising beam splitter (PBS), which transmit and reflect orthogonally polarised electric field components (horizontal and vertical), with each beam being measured by separate detectors. The PPBS, quarter-wave plate (QWP) and half-wave plate (HWP) serves to split the sampling light input such that the detectors will measure the polarisation input using four Stokes vectors, that maps a tetrahedron on a Poincaré sphere, as calibration basis vectors. It can be shown that as long these Stokes vectors form a tetrahedron, regardless of the orientation, it will give the least uncertainty in polarisation measurement [18, 17, 19, 20].

Again, the whole measurement process can be represented as a matrix manipulation. The polarimeter can be represented by an 4-by-4 instrument matrix, \mathbf{I} that transforms the normalised Stokes vector into a 4-by-1 matrix comprising of the readings of each of the detector

$$\mathbf{I} \begin{pmatrix} 1 \\ S_1/S_0 \\ S_2/S_0 \\ S_3/S_0 \end{pmatrix} = \begin{pmatrix} D_1 \\ D_2 \\ D_3 \\ D_4 \end{pmatrix} \quad (2.16)$$

It should also be noted that the detector readings D_1 , D_2 , D_3 and D_4 are normalised to the total readings measured by all 4 detectors. The instrument matrix will again be of use in the later part of the report.

Chapter 3

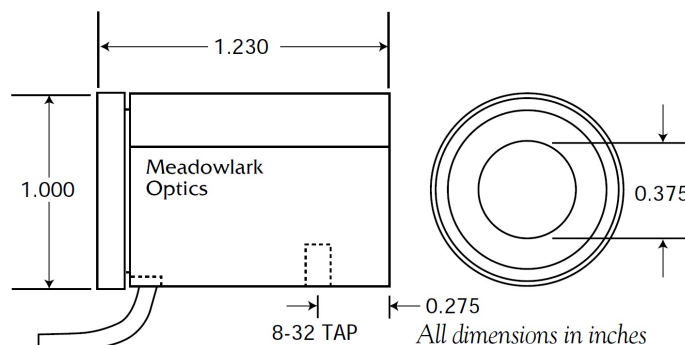
Experiment and Methodology

We use an industrial standard telecommunication wavelength [21, 22], 1310nm as the choice for this project. This is because the polarisation compensation scheme is targeted at commercial QKDs which will likely be operated by telecommunications companies.

The light source that we will be using is a commercial single mode distributed feedback (DFB) laser diode from Thorlabs Inc (Model LP1310-SAD2) with a centre wavelength of 1310nm [23].

In this experiment, any polarisation mentioned thereafter is defined with respect to the lab frame. That is, the horizontal basis is defined to be parallel to the optical bench surface.

3.1 Characterisation of Liquid Crystal Variable Retarders



- (i) Photograph of the Meadowlark Optic's liquid crystal variable retarder mounted on a rotatable mount. (ii) Side and front drawing of the liquid crystal and its dimensions. Picture taken from [2]

Figure 3.1: Meadowlark Optic's liquid crystal variable retarder

The liquid crystal variable retarder (LCVR) was mentioned in Section 2.2.2 and we will be using Meadowlark Optic's nematic liquid crystal (Model LRC-100-IR3 [2]). We managed to characterise three of such LCVRs, the results for the first one is show here while the second and third one is attached in Appendix A.

To characterise the LCVR, we first set up a crossed polariser as shown in Figure 3.2 to determine it's optical axis.

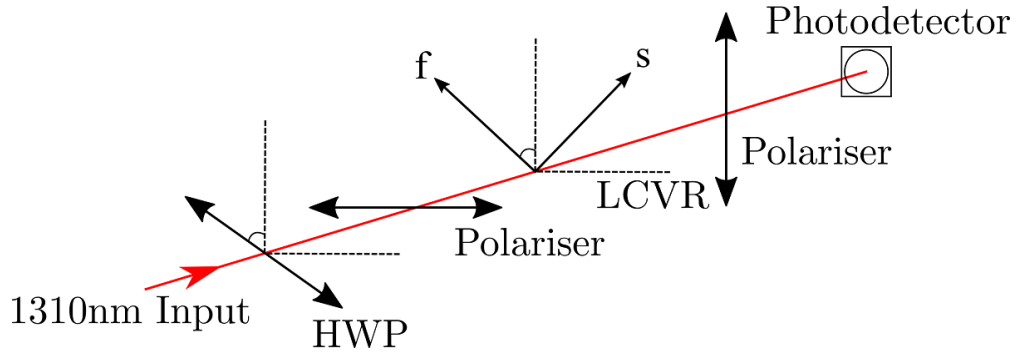


Figure 3.2: Schematic of the crossed polariser set-up.

The crossed polariser set-up consists of two linear polarisers with their optical axis perpendicular to each other. In Figure 3.2, an additional half-wave plate was added before the first linear polariser (horizontal transmission axis) to maximise the input transmission through the horizontal axis. Without the LCVR in between the crossed polarisers, we would expect that the output intensity at the photodetector in the ideal situation to be minimised, since the two polarisers are crossed. With an LCVR added in between the two crossed polarisers, the horizontally polarised input can be altered according to the angle of its optical axis and its retardance.

However, when the optical axis of the LCVR is aligned to the vertical or horizontal linear polariser, no change in retardance will affect the polarisation. This is when we know the LCVR optical axis is aligned to the horizontal or vertical axis.

A photodetector is positioned at the end of the crossed polariser set-up. The LCVR is mounted on a rotatable mount and is rotated such that the photodetector shows a minimal intensity reading. This position will be marked as its optical axis.

We continue to use the same crossed polariser set-up as shown in Figure 3.2. However, we rotate the LCVR such that its optical axis is now angled 45° with respect to the optical axis of both the crossed polarisers. At this position, we vary the voltage input of the LCVR and measure the intensity of light on the photodetector of the set-up. This process will allow us to characterise the retardance of the LCVR.

The LCVR operates with a 2 kHz square wave alternating voltage input. The voltage input refers to the peak voltage, V_{pk} . An oscilloscope image of the waveform generated by the function generator is shown in Figure 3.3.

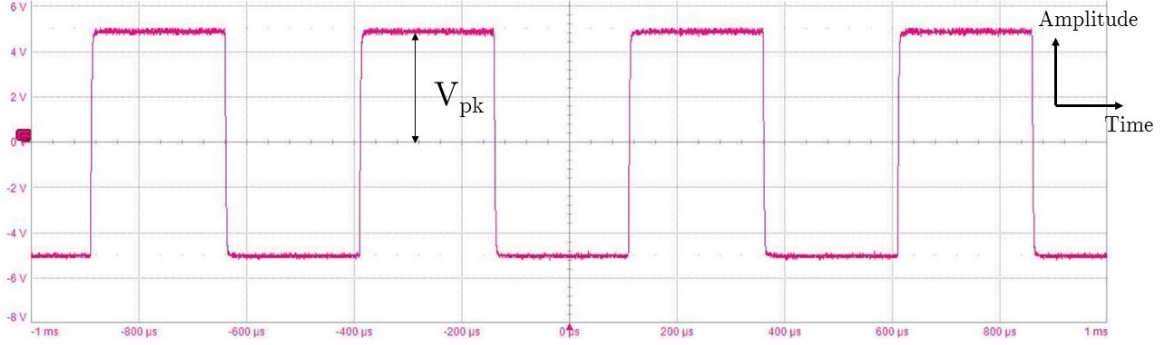


Figure 3.3: Generated voltage waveform used to control the LCVRs.

To understand the characterisation process, we return to the Mueller matrix of the variable retarder in Section 2.2.2. In this case, we substitute $\theta = 45^\circ$ and operate the matrix on the horizontally polarised input light

$$\begin{pmatrix} 1 & 0 & 0 & 0 \\ 0 & \cos(\phi) & 0 & -\sin(\phi) \\ 0 & 0 & 1 & 0 \\ 0 & \sin(\phi) & 0 & \cos(\phi) \end{pmatrix} \begin{pmatrix} 1 \\ 1 \\ 0 \\ 0 \end{pmatrix} = \begin{pmatrix} 1 \\ \cos(\phi) \\ 0 \\ \sin(\phi) \end{pmatrix} \quad (3.1)$$

which after the linear polariser with axis set to vertical, we obtain

$$\frac{1}{2} \begin{pmatrix} 1 & -1 & 0 & 0 \\ -1 & 1 & 0 & 0 \\ 0 & 0 & 0 & 0 \\ 0 & 0 & 0 & 0 \end{pmatrix} \begin{pmatrix} 1 \\ \cos(\phi) \\ 0 \\ \sin(\phi) \end{pmatrix} = \frac{1}{2} \begin{pmatrix} 1 - \cos(\phi) \\ -1 + \cos(\phi) \\ 0 \\ 0 \end{pmatrix} \quad (3.2)$$

If one normalises the final Stokes vector in Equation 3.2 with the first component of the resulting matrix ($\frac{1 - \cos(\phi)}{2}$), the second component will always be -1 except for the case of $\phi = 0$, which is what we expect from the output after a linear polariser with axis set to vertical.

The first component reflects the intensity the photodetector will measure and is also scaled to the transmittance. If we consider the maximum transmittance, T_{max} which occurs at $\phi = \pi$, the transmittance function, $T(\phi)$ is simply the product between the first component ($\frac{1 - \cos(\phi)}{2}$) and maximum intensity reading

$$T(\phi) = \frac{1 - \cos(\phi)}{2} T_{max} \quad (3.3)$$

As $T(\phi)$ is directly proportional to the photodetector reading, $V(\phi)$ we only need to simply rearrange the equation to arrive at

$$\phi = \cos^{-1}\left(1 - \frac{2V(\phi)}{V_{max}}\right) \quad (3.4)$$

Where we have replaced T_{max} with V_{max} , the maximum voltage reading from the photodetector. This will be the equation used to characterise the LCVRs.

We vary the peak voltage input to the LCVR, V_{pk} in steps of 0.05V between 0V to 10V and recorded the voltage reading from a photodetector. At each voltage input setting, we recorded 200 points of photodetector voltage readings. The mean is then plot against the LCVR voltage input as shown in Figure 3.4. However, we also have to account for the intrinsic noise of the photodetector which contributes to both random and systematic errors on the voltage readings.

The intrinsic noise of the photodetector is determined by the minimum from the mean of the voltage reading at each LCVR voltage input (This occurs when the retardance of the LCVR is zero and the intensity output should be zero). The mean data is then normalised to this minimum and is then used to calculate the retardance using Equation 3.4 and the results for the same LCVR is shown in Figure 3.5.

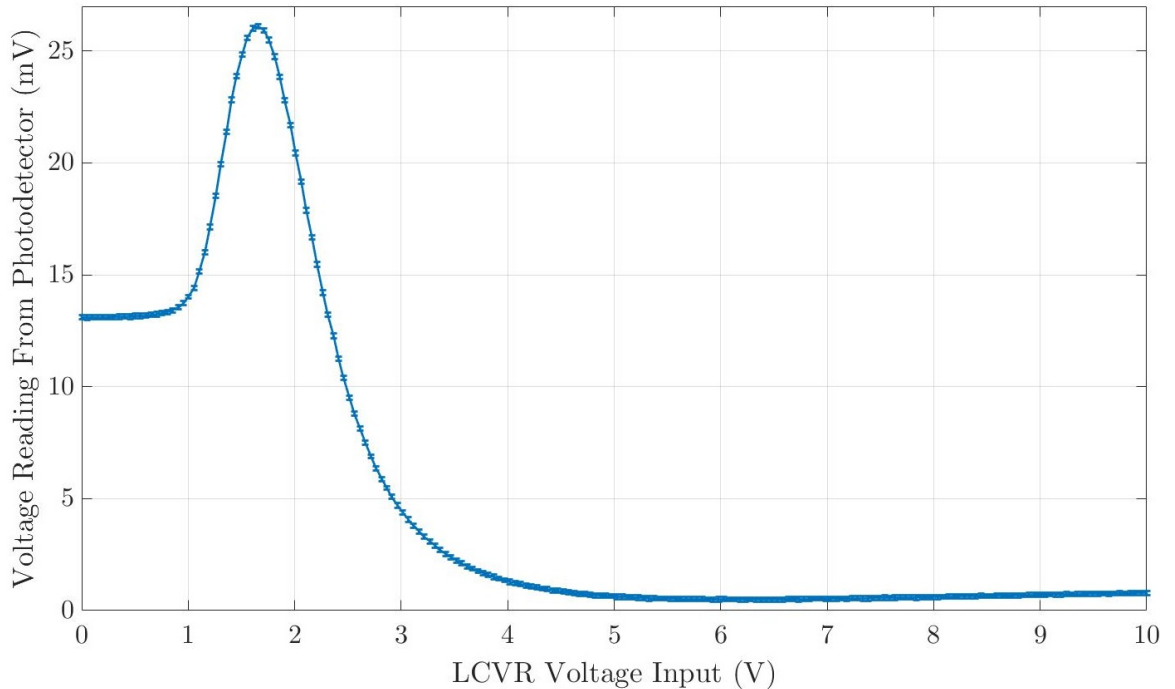


Figure 3.4: Plot of mean raw voltage reading of photodetector vs LCVR voltage input for crossed polariser set-up in Figure 3.2.

The error bars are of 1 standard deviation value and are due to the random fluctuations of the intrinsic noise of the photodetector. We first notice that the error bars are significantly larger at the region when the photodetector voltage is close to zero in Figure 3.4. Since this is primarily due to the intrinsic noise of the photodetector that contributes to random errors, this voltage readings fluctuates significantly due to the now comparable noise level when the photodetector voltage is close to zero. We also note that the retardance range of the LCVR varies approximately between 0 to $\frac{3\pi}{2}$ and that this range can be utilise with voltage input between $\sim 1\text{V}$ to 6V .

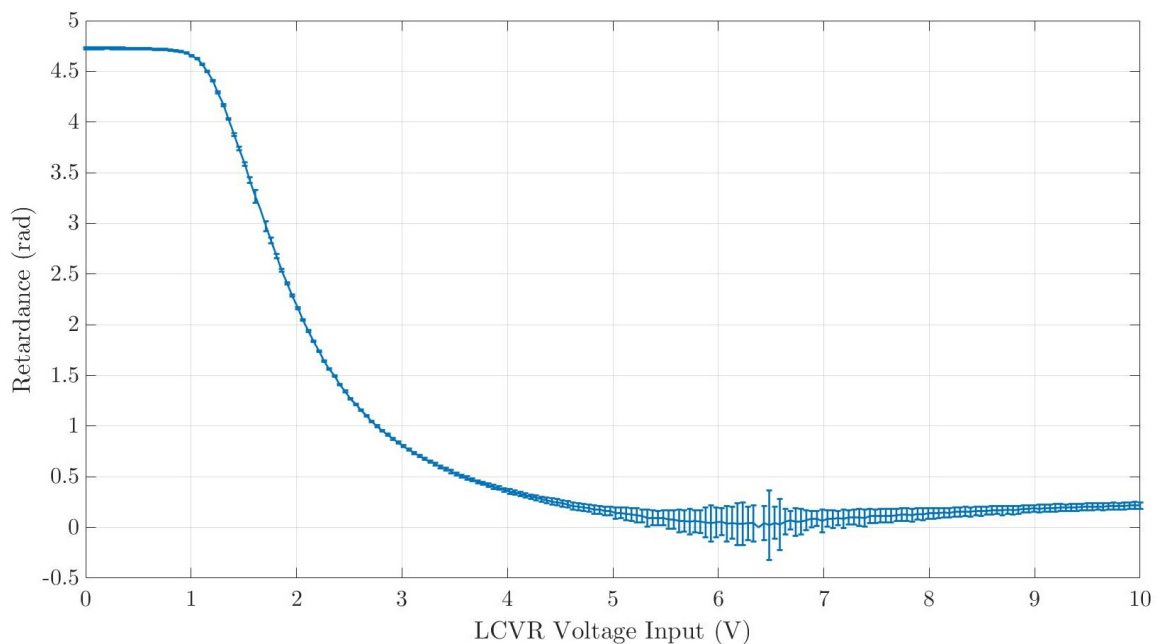


Figure 3.5: Plot of LCVR retardance vs LCVR voltage input.

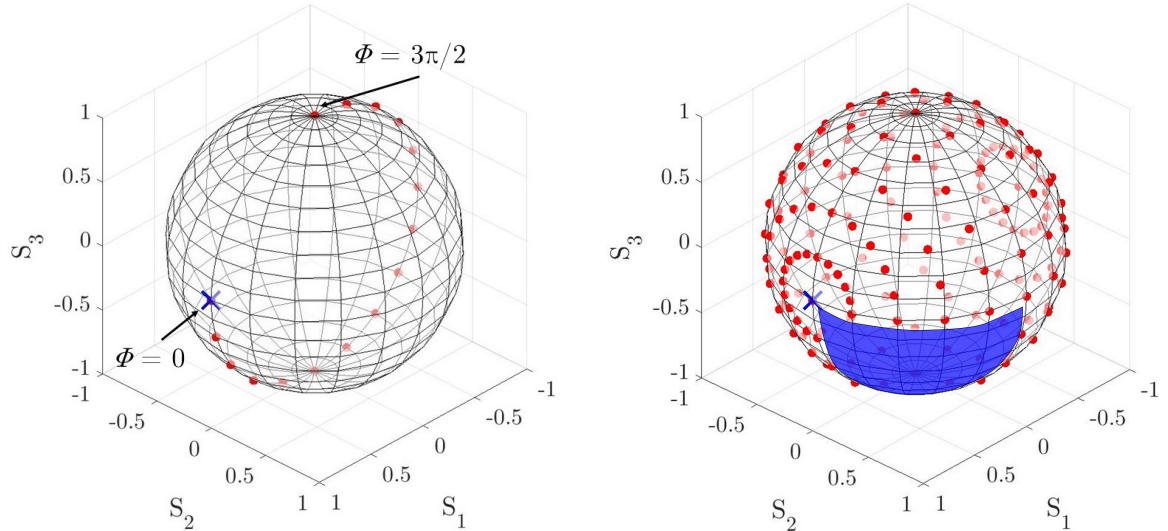
3.2 Polarisation Control Using LCVRs

With the optical axis of the LCVR determined and its retardance range quantified, we now simulate the extent of polarisation states coverage that can be achieved by different number of LCVRs in an array.

First we consider a LCVR with its optical axis angled 45° to the horizontal with an incident horizontal polarised light. Given that the retardance range of LCVR is between 0 to $\frac{3\pi}{2}$, the possible output polarisation states will trace an arc across the Poincaré sphere from the equator to the pole, then to the equator and to the opposite pole as shown in Figure 3.6(i).

For the purpose of polarisation compensation, one LCVR is not enough. The ideal situation would be to have an configuration of multiple of LCVRs that can alter the

input polarisation state to all other polarisation states. Thus, by adding one more LCVR with its optical axis aligned to the horizontal, we obtain a larger coverage as shown by the area covered by the red points in Figure 3.6(ii), which is more promising for the purpose of polarisation compensation. Only a quadrant of the Poincaré sphere is not covered as highlighted by the blue region.



(i) Polarisation transformation coverage by a LCVR with retardance varying from $\phi = 0$ to $\frac{3\pi}{2}$.

(ii) Polarisation transformation coverage by 2 LCVRs. The blue shaded region is inaccessible.

Figure 3.6: Poincaré sphere diagrams of LCVR coverage.

However, we also need to consider other cases where the input polarisation is not horizontal. Suppose the input polarisation fluctuates to an extent where it becomes aligned to the initial LCVR, then there is one degree of freedom less to compensate drift. This is similar to the gimbal lock problem.

Gimbal lock occurs when a three-dimensional, three-gimbal mechanism has two of its gimbals rotating in the same axes which as a result causes an effective reduction of degrees of freedom by one. The most direct solution is to add a fourth gimbal that is actively corrected to provide another degree of freedom of rotation [24].

The most direct solution to mitigate the above situation is to add more LCVRs, each angled 45° to one another. In this context, we will need four LCVRs lined up as shown in Figure 3.7. Even with at the gimbal lock situation, it still can transform the polarisation states sufficiently across the Poincaré sphere.

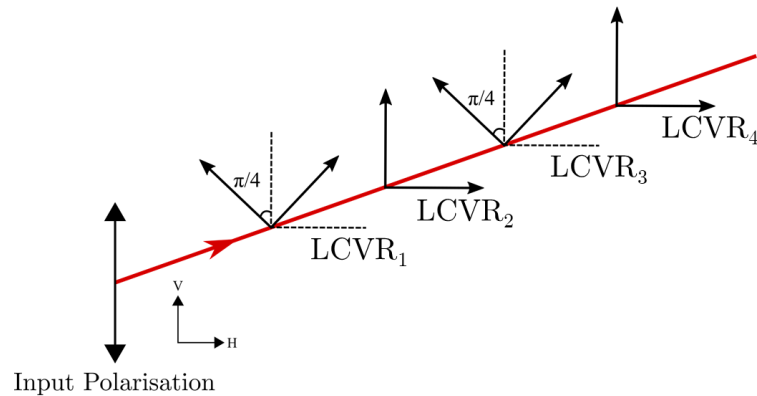
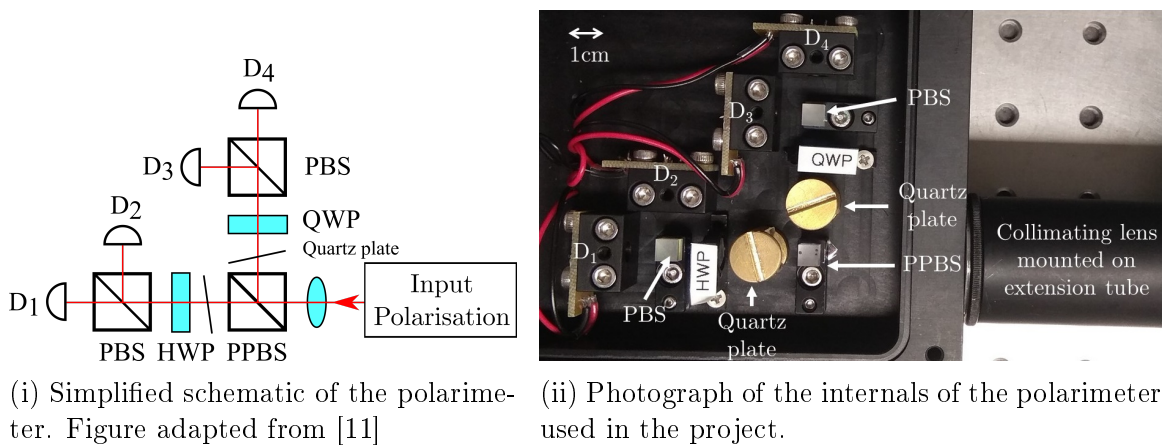


Figure 3.7: Simplified schematic of an array of four LCVRs.

3.3 Setting Up The Polarimeter

In this section, we detail the set up and characterisation of the aforementioned polarimeter. A picture of the actual device is shown in Figure 3.8(ii) and quartz plates have been introduced. The quartz plates serve to correct for phase shift induced by the non-ideal partially polarising beam splitter [11].



(i) Simplified schematic of the polarimeter. Figure adapted from [11]

(ii) Photograph of the internals of the polarimeter used in the project.

Figure 3.8: Polarimeter.

The purpose of characterising the polarimeter is to find the instrument matrix representing itself. Essentially, the optimal instrument matrix can be determined as long we choose four calibration states that are spread out significantly on the Poincaré sphere to form, as close as possible, a tetrahedron. From Equation 2.16, the

instrument matrix can be expressed as

$$\mathbf{I} = \begin{pmatrix} D_1 \\ D_2 \\ D_3 \\ D_4 \end{pmatrix} \begin{pmatrix} 1 \\ S_1/S_0 \\ S_2/S_0 \\ S_3/S_0 \end{pmatrix}^{-1} = {}^{(1)}\vec{D} {}^{(1)}\vec{S}^{-1} \quad (3.5)$$

However, as the instrument matrix is a 4-by-4 matrix with 16 unknown components, we will need four sets of four simultaneous equations to solve the matrix. To do that, we need 4 calibration states, ${}^{(1)}\vec{C}$, ${}^{(2)}\vec{C}$, ${}^{(3)}\vec{C}$ and ${}^{(4)}\vec{C}$, and solve the equation

$$\mathbf{I} = \begin{pmatrix} {}^{(1)}\vec{D} & {}^{(2)}\vec{D} & {}^{(3)}\vec{D} & {}^{(4)}\vec{D} \end{pmatrix} \begin{pmatrix} {}^{(1)}\vec{C} & {}^{(2)}\vec{C} & {}^{(3)}\vec{C} & {}^{(4)}\vec{C} \end{pmatrix}^{-1} \quad (3.6)$$

The determination of the calibration states will be a trial and error process using the following experimental set-up.

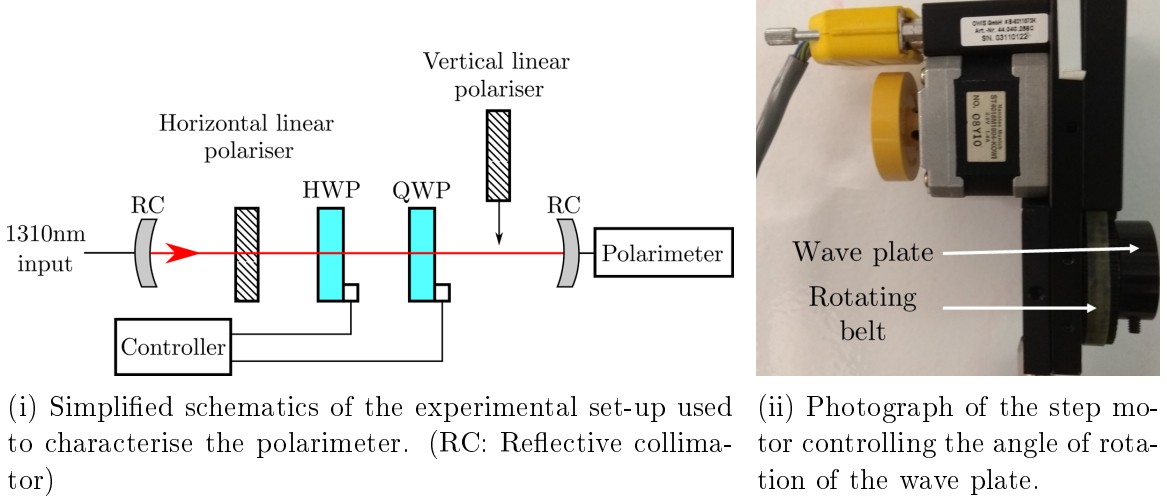


Figure 3.9: Polarimeter characterisation set-up schematic.

A crossed polariser set-up is used initially to determine the optical axis of the half-wave plate (HWP) and quarter-wave plate (QWP). The process is the same as in Section 3.1 where we described the process of determining the optical axis of the LCVR. However, in this case, the HWP and QWP are mounted on a step motor as shown in Figure 3.9(ii) which is controlled by a computer.

After the optical axes are determined, the vertical linear polariser is removed. At this stage, we send horizontally polarised 1310nm light through the step motor mounted wave plates. As discussed earlier in Section 2.2.1, the wave plates can alter the polarisation state of the 1310nm light input. By varying the angles of both wave

plates using the step motor, we can generate all possible polarisation states that covers the entire surface of a poincaré sphere.

We first configure 2025 known polarisation states with the step motor mounted wave plates and send them in one by one into the polarimeter. The detector readings are then recorded and normalised to the total reading. To ensure that the phase induced by the PPBS is minimised, the quartz plates are adjusted by means of trial and error. This is done by rotating its mounts in small steps to vary the angle of incidence of the daughter beams from the PPBS. If the quartz plates are not adjusted correctly, the calibration states will not form a tetrahedron properly and will tend to lie on the same plane. As a result, the accuracy of reconstructing the Stokes vector by the instrument matrix is poor.

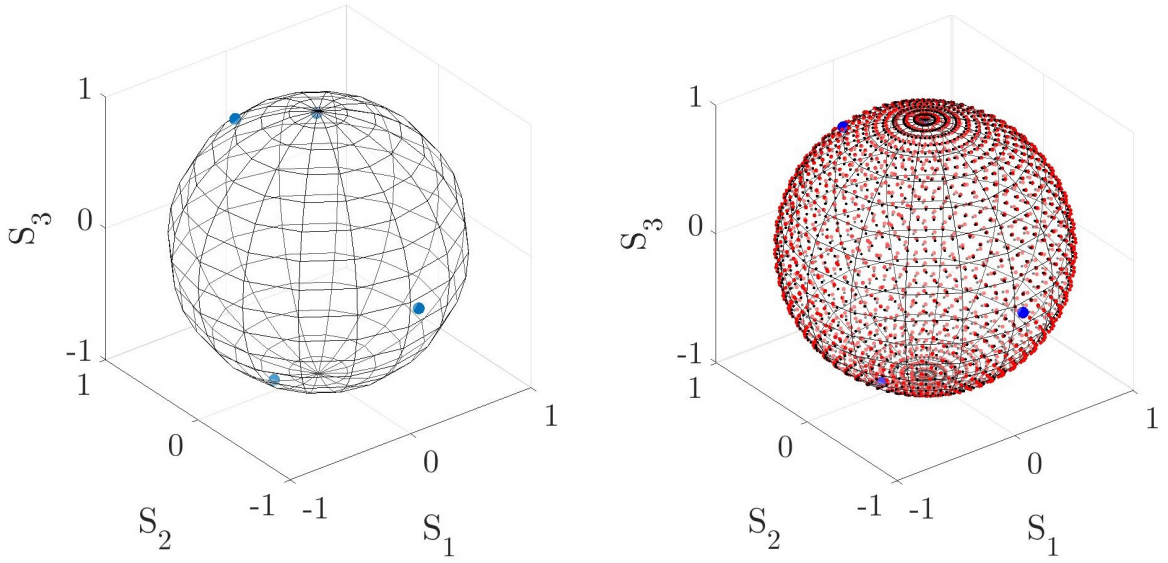
After a data of 2025 readings is recorded, we determine the calibration Stokes vector out of the 2025 by means of selecting those corresponding reading sets which has a maximum reading for one of the detector, i.e.

$${}^{(1)}\vec{C} \rightarrow {}^{(1)}\vec{D} = \begin{pmatrix} {}^{(1)}D_1 \\ {}^{(1)}D_2 \\ {}^{(1)}D_3 \\ {}^{(1)}D_4 \end{pmatrix}$$

where ${}^{(1)}D_1$ is the highest reading for detector 1 (see Figure 3.8(i)) out of the 2025 reading sets and

$${}^{(2)}\vec{C} \rightarrow {}^{(2)}\vec{D} = \begin{pmatrix} {}^{(2)}D_1 \\ {}^{(2)}D_2 \\ {}^{(2)}D_3 \\ {}^{(2)}D_4 \end{pmatrix}$$

where ${}^{(2)}D_2$ is the largest reading for detector 2 (see Figure 3.8(i)) out of the 2025 reading sets and so forth for the third and fourth calibration states.



(i) The four calibration Stokes vectors quite spread apart although not optimally a tetrahedron yet.

(ii) The black dots represent the 2025 known input polarisation states while the red dots represent the reconstructed Stokes vectors using the instrument matrix. The larger blue dots are the calibration Stokes vectors

Figure 3.10: Reconstruction of the Stokes vectors using the instrument matrix determined by the calibration states as shown on the Poincaré sphere.

By varying the angle of the quartz plates, we attempt to achieve the configuration such that the calibration Stokes vector are spread apart as much as possible to form a tetrahedron. Once a reasonable result is achieved, as shown in Figure 3.10(i), we collated 33 sets of data and used the mean of the readings to determine the instrument matrix. The instrument matrix is determined to be

$$\mathbf{I} = \begin{pmatrix} 0.19252 & -0.04991 & 0.09237 & 0.16034 \\ 0.24557 & 0.13676 & 0.17461 & 0.10545 \\ 0.27021 & -0.09427 & 0.01086 & -0.25456 \\ 0.29170 & 0.00742 & -0.27784 & -0.01122 \end{pmatrix} \quad (3.7)$$

The 2025 normalised mean detector readings are processed with the derived instrument matrix in Equation 3.7 to generate reconstructed Stokes vectors (red dots in Figure 3.10(ii)) and are plotted on the Poincaré sphere as shown in Figure 3.10(ii) with the original polarisation states input (black dots in Figure 3.10(ii)). The fidelity appears reasonable to a good degree and for the purpose of this experiment, is accurate enough. Further analysis of the data is attached in Appendix B.

For any subsequent polarimeter reading, the corresponding Stokes vector can be

determined by

$$\vec{S} = \mathbf{I}^{-1}\vec{D} \quad (3.8)$$

Where

$$\mathbf{I}^{-1} = \begin{pmatrix} 1.00000 & 1.00000 & 1.00000 & 1.00000 \\ -5.11178 & 4.39761 & 1.00783 & -1.44255 \\ 0.79264 & 1.18821 & -2.54579 & 1.10367 \\ 2.98828 & -0.51640 & 0.57964 & -2.28559 \end{pmatrix} \quad (3.9)$$

Chapter 4

Results and Analysis

With the instrument matrix of the polarimeter determined, we can now quantify the polarisation drift that we aim to compensate. For this project, we will be using a 1km long SMF28e+ optical fibre spool [25] as a test subject to simulate the polarisation drift. A simplified schematic of the toy model is shown in Figure 4.1.

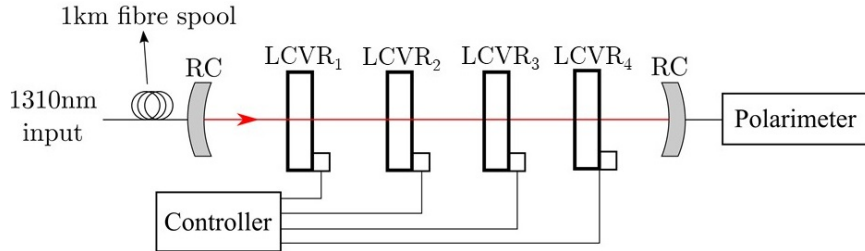


Figure 4.1: Schematic of the toy model used to simulate polarisation drift.

4.1 Measuring Polarisation Drift

The polarisation was monitored with a 1310nm laser input (Model: Thorlabs LP1310-SAD2 [23]) with power output maintained at 2.4mW by the laser controller (Model: Thorlabs ITC4001 [26]) and beam waist of 2mm. The laser diode's temperature is maintained at 35°C by the thermoelectric cooler (TEC). After coupling the input into the polarimeter (without the LCVRs), the transmission efficiency registered is about 55% at ~ 1.3 mW. With the the four LCVRs, the overall transmission efficiency is about 25%. While the lost in power is significant, the overall power output is still sufficient for the compensation test. Further optimisation process such as better optical alignment could have been done to increase the transmission efficiency.

We first monitor the polarisation output from the spool of 1km optical fibre spool without the LCVRs. The optical fibre spool is placed on four posts support and is

left untouched. The polarimeter is set to take readings in intervals of 1s. The process lasted about 48 hours and the polarisation readings are shown in both Figure 4.2 and 4.3.

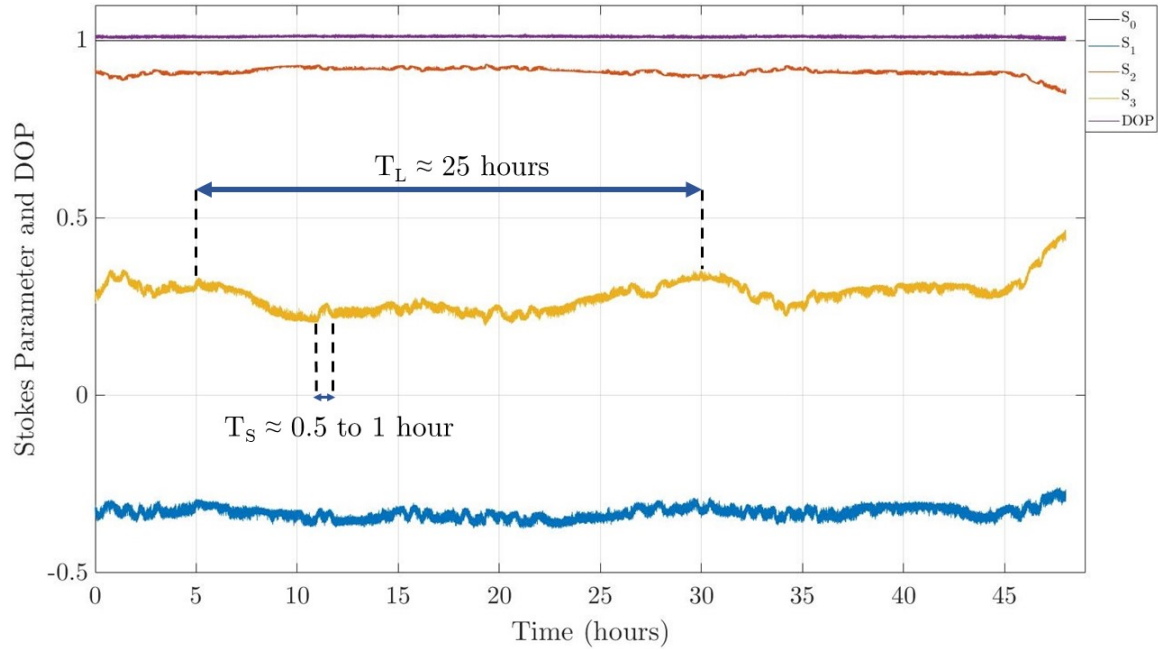
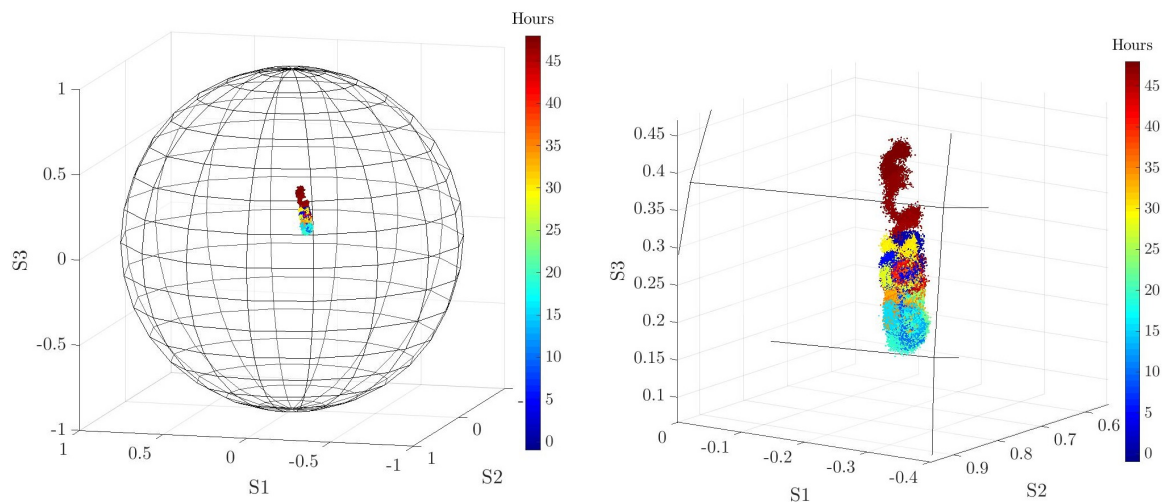


Figure 4.2: Plot of Stokes parameters and degree of polarisation (DOP) of the laser output vs time to show fluctuation in polarisation across the 1km fibre spool.



(i) Polarisation state of the output after the 1km fibre without the LCVRs monitored over 48 hours.

(ii) A closer view of the polarisation drift over time from Figure 4.3(i).

Figure 4.3: Polarisation drift across the 1km fibre spool visualised on a Poincaré sphere.

Observing the fluctuation of the Stokes parameters in Figure 4.2, we notice that there are noticeable fluctuations across the three Stokes parameters, especially S_3 . We also note that the polarisation output is elliptical. A large and relatively slow drift of magnitude $\Delta S_3 \sim 0.1$ with a period of about a day as labelled by T_L is shown in Figure 4.2. In addition, a smaller and relatively faster drift of magnitude $\Delta S_{1,2,3} \sim 0.05$ with a period of about an hour as labelled by T_S in Figure 4.2 can be observed across all three Stokes parameters. As for the degree of polarisation (DOP), it is generally close to 1 over the entire measurement period. The fluctuation as characterised by T_L is likely due to the temperature fluctuation of the laboratory.

From Figure 4.3, the plot of the polarisation states on the Poincaré also give us a better picture of the extent of the polarisation fluctuations. In general, we note that the drift is mostly confined to a small area which means that the compensation set up with 4 LCVRs is able to provide enough coverage to perform the compensation for the toy model.

We further observe the polarisation drift in a smaller time scale of 1 hour.

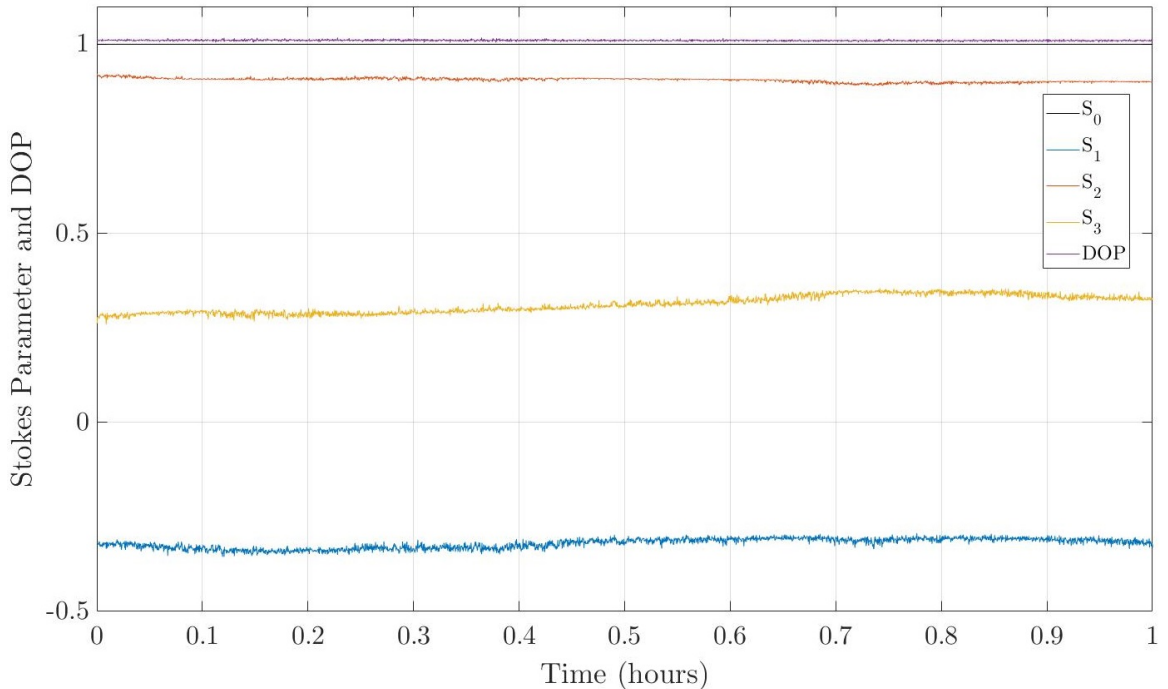


Figure 4.4: Plot of Stokes parameters and DOP vs time in 1 hour to show fluctuation in polarisation across the 1km fibre spool.

From Figure 4.4, we notice that the readings are rather noisy with fluctuation on the order of ~ 0.01 , mainly due to the noise from the polarimeter detectors. However,

such fluctuations are still acceptable within this experiment context as the magnitude of fluctuation is small ($\pm 1\%$). Other than S_3 which shows a more significant fluctuation in value, the other Stokes parameters are reasonably consistent.

We also note that the results were obtained in laboratory settings through a 1km optical fibre spool where environmental conditions are relatively stable. In a realistic context where optical fibres are laid underground on a city scale (10-100km fibre length), we expect even a greater degree of fluctuation in polarisation. This is because the temperature changes in the ground are greater than in the lab and mechanical vibrations due to traffic are likely to further contribute to the amount of polarisation drift.

As an additional investigation, we also tested the constant current mode on the laser controller. In this mode, the laser diode current is kept constant instead it's power output. The polarisation is monitored over a period of about 25 hours and the data is left in Appendix C. There is no significant difference in polarisation fluctuation between these two laser driving modes.

4.2 Polarisation Compensation Results

We placed the LCVRs back into the set-up as described in Figure 4.1 and 3.7 to test the polarisation drift compensation code. The code, attached in Appendix D, is based on the gradient descent algorithm [27] which uses an optimisation technique to solve for conditions such as minimums in functions. It works in the following manner:

1. The desired polarisation state is set first, which is the horizontal polarisation state in our test.
2. The LCVR voltages are all set to 3.5V (Somewhere in between its operation range as described in Section 3.1).
3. The polarisation state is sampled approximately in intervals of approximately 0.1s.
4. The error between the measured polarisation and desired polarisation state is measured. Then the correction step begins.
5. The first LCVR voltage input is increased by a small step. If the error increases, we decrease the voltage input. If decreasing the voltage input still increases the error, we reset back to the original voltage input in this correction step.

6. The above step is repeated for the next three LCVRs
7. The voltage adjustments in step 5 and 6 are repeated in subsequent correction step until the error is below a certain threshold.

Suppose the desired polarisation state is \vec{S} and the measured polarisation state is \vec{S}' , the error, which we defined as a root mean squared value, E is quantified as such:

$$E = \sqrt{(S_1 - S'_1)^2 + (S_2 - S'_2)^2 + (S_3 - S'_3)^2} \quad (4.1)$$

A quick analysis of Equation 4.1 will tell us that $E = 0$ corresponds to no error between the measured and desired polarisation while $E = 2$ corresponds to the highest error when the measured state is orthogonal to the desired state. We have set the error threshold to be 0.015. This is because of the imperfection of the instrument matrix of the polarimeter and also polarisation of light. From Figure 4.3, we see that the degree of polarisation is consistently more than the maximum of 1, at approximately 1.01 to 1.02. Hence, any polarisation measured will always have at least an error of approximately 0.01 to 0.02. Thus, the baseline of the error is set at 0.015.

The LCVR voltage input change is set at $\Delta V = 0.03$ to make minute adjustments to the retardance of the LCVRs but not too small such that it takes unnecessarily long for the compensation to be done. To prevent the compensation code from adjusting the LCVR voltage input such that it exceeds the operational retardance range of the LCVRs, a lower and upper limit of 1.0V and 6.0V is set respectively. If the voltages reaches such limits, the compensation code will reset it to the starting operating voltage of 3.5V.

Applying the aforementioned code, we proceed to monitor the polarisation output over a period of over 6 hours. The Stokes parameters are shown in Figure 4.5 and are plotted on the Poincaré sphere in Figure 4.7. We also notice from Figure 4.9 that the time taken for the polarisation drift compensation code to correct the initial elliptical polarisation (closer to -45°) to as close to the desired horizontal polarisation state within the error threshold to be 81.1s. The active polarisation compensation code appears to be working consistently for the remaining duration of the test with a time average error of $\mathbf{E} = 0.01501 \pm 0.01194$ after the 81.1s mark.

We have also included the voltage input to the four LCVRs over time in Figure 4.8 and 4.9.

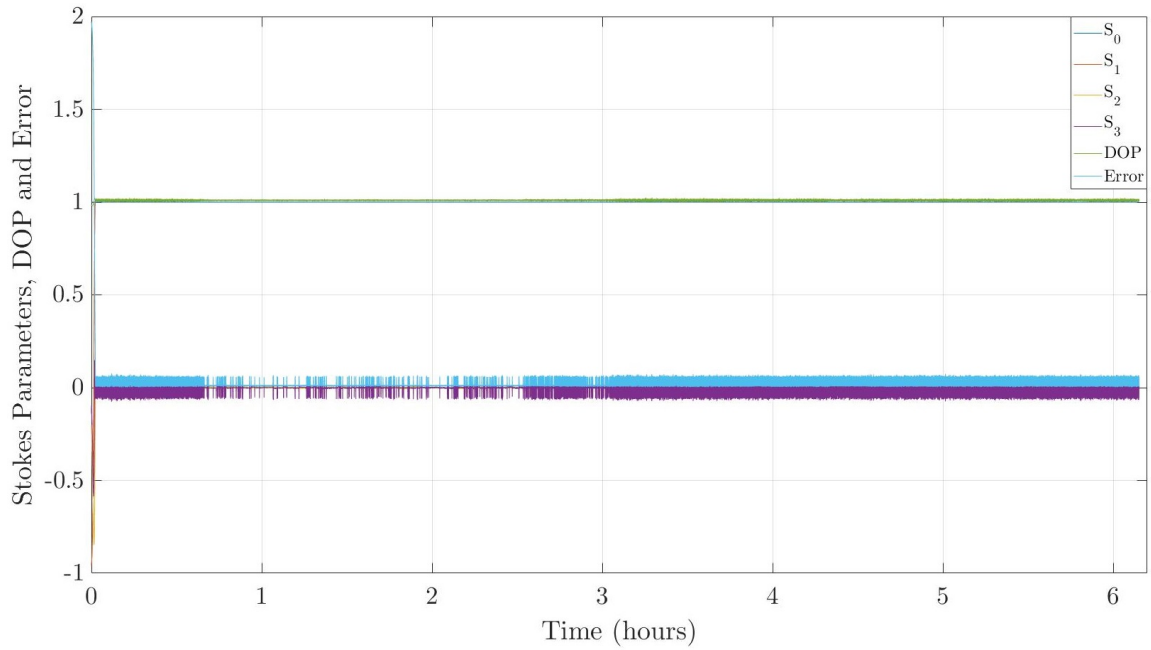


Figure 4.5: Plot of Stokes parameters, DOP and Error vs time of polarisation across the 1km fibre spool but with active polarisation compensation code running.

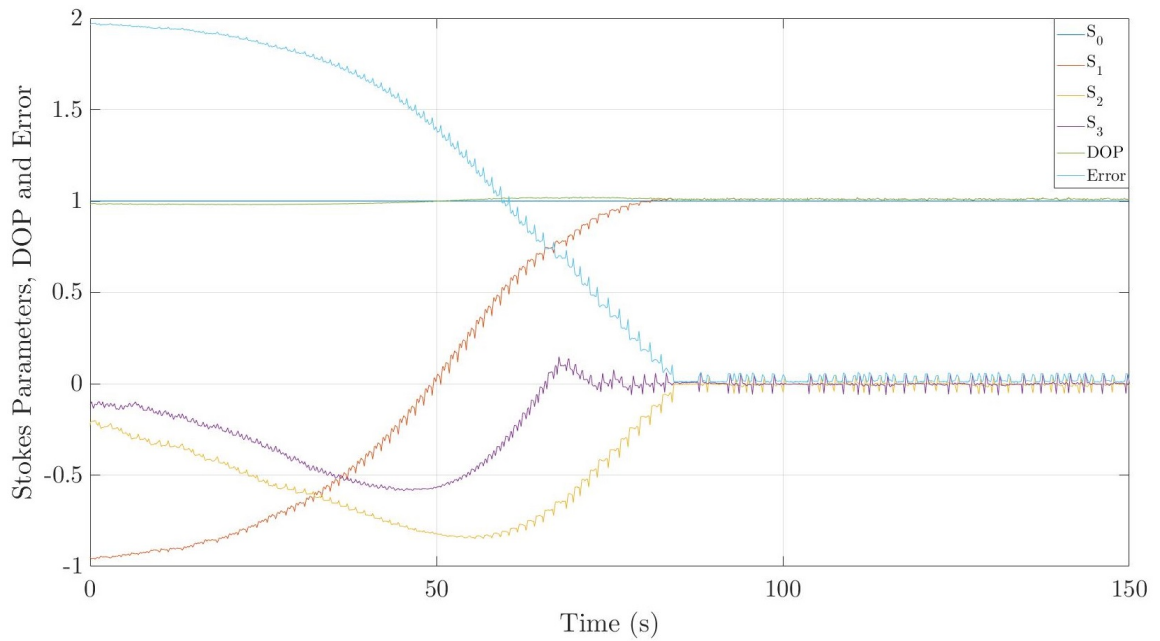
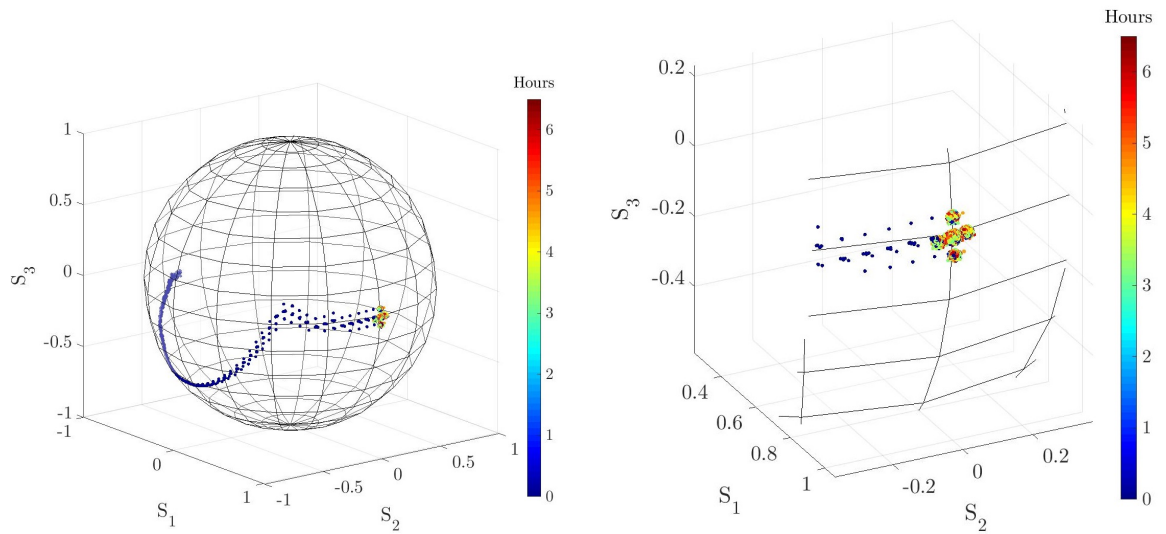


Figure 4.6: Plot of Stokes parameters, DOP and Error vs time for the first 150s of polarisation output across the 1km fibre spool with active polarisation compensation code running.



(i) Polarisation state of the output after the 1km fibre with the LCVRs and active polarisation compensation monitored over 6 hours.

(ii) A closer view of the polarisation output over time from Figure 4.7(i).

Figure 4.7: Polarisation output across the 1km fibre spool with active polarisation compensation visualised on a Poincaré sphere.

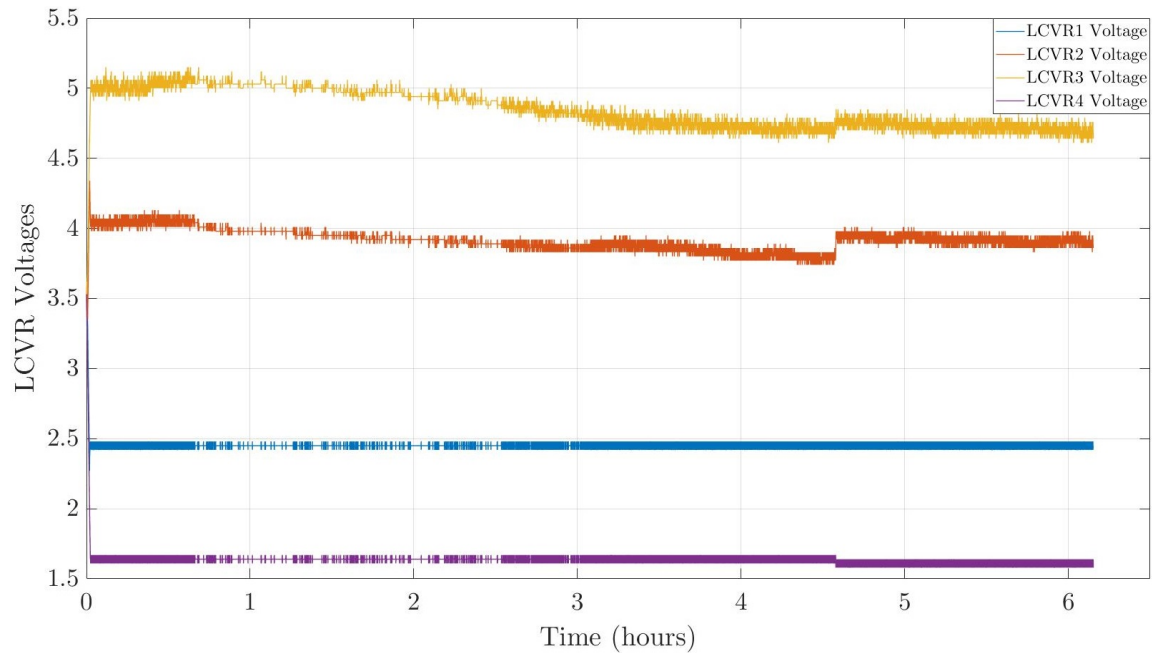


Figure 4.8: Plot of LCVR voltage inputs vs time of polarisation output across the 1km fibre spool with active polarisation compensation code running.

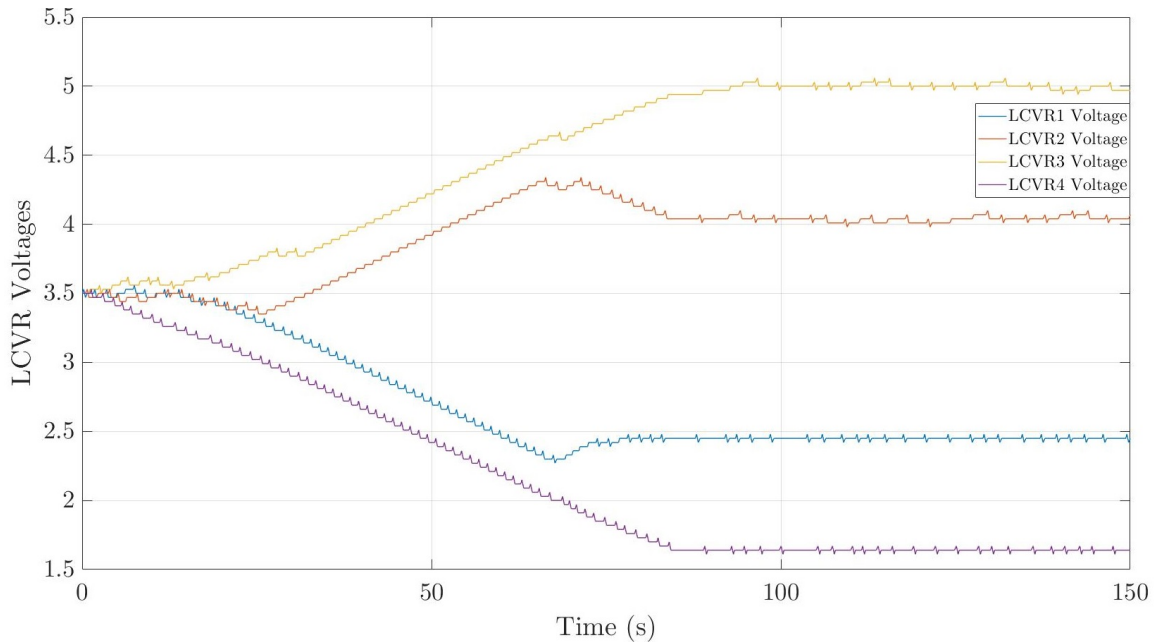


Figure 4.9: Plot of LCVR voltage inputs for the first 150s of polarisation output across the 1km fibre spool with active polarisation compensation code running.

From Figure 4.9, we can observe how the polarisation compensation code adjusts the LCVRs voltage input in small steps until the desired polarisation state is reached. We can see from Figure 4.8 that for the remaining period, constant small adjustments are continuously added to maintain the polarisation output as close as possible to the desired state. As a result, the constant polarisation fluctuation and adjustments contributed to the spiky appearance of Figure 4.5, 4.6, 4.8 and 4.9. This fluctuation could have also been due to the intrinsic noise of the photodetectors.

We also observe from Figure 4.7(i) that the LCVRs array provided enough coverage to alter the polarisation output across about a quadrant of the Poincaré sphere surface. This is a promising result to show that the array configuration is indeed able to provide sufficient coverage across the Poincaré sphere as discussed in Section 3.2.

Due to time constrain, we managed to only test the code for a duration of over 6 hours. Longer periods of tests could have been ran to determine the maximum durability of the code. However, we are now confident that the set-up can compensate for drifts in the order of $T_S \simeq 0.5$ to 1.0 hour as described in Figure 4.2.

Chapter 5

Conclusion and Further Discussions

We have shown preliminary work that the polarisation drift compensation scheme we have devised is able to operate within the threshold we have set in this project. It is able to effectively to correct polarisation drifts with periods on the order of 1 hour and is able to consistently compensate for at least 6 hours.

While preliminary results from this project suggests valuable potential of the compensation scheme, more rigorous tests are needed to check its feasibility in implementing it in a commercial QKD. For one, we were unable to correct the fast fluctuation that are a result of the intrinsic noise of the photodetectors of the polarimeter. One way to mitigate this technical issue is to further characterise the polarimeter in detail, such as accounting for the intrinsic noise and to further optimise the angle of the quartz plates to correct for the phase induced by the PPBS. Even with this factor accounted, we cannot neglect the possibility of polarisation fluctuations that occurs on the order of minutes or seconds which we did not consider or investigate in further detail in this project.

The polarisation compensation code can also be further improved to have faster and more efficient (less correction steps) response. For example, instead of large amounts of small correction steps, the algorithm can be modified to find a fastest way to change the LCVRs voltage input altogether to minimise the error in the shortest time possible.

We could also have investigated in detail the causes of polarisation fluctuations and their effects. For example, in Figure 4.2 we notice that only the parameter S_3 is being affected more than the other 2 Stokes parameters.

Further tests and optimisation are required for the polarisation drift compensation schemes to prove their validity in commercial QKD. For example, instead of using our own definition of error as the basis for compensation, we could also use polarisation correlation, viability measurement or Bell variables as our scale for error measurement.

Appendix A

Characterisation of Liquid Crystal Variable Retarders

The data acquired from the characterisation of the second and third liquid crystal variable retarders (LCVR) are contained in this appendix (Note that the fourth LCVR is not characterised due to time constrain). Note that the retardance range of the two LCVRs were roughly the same. The set-up that is used is described in Section 3.1 and shown in Figure 3.2.

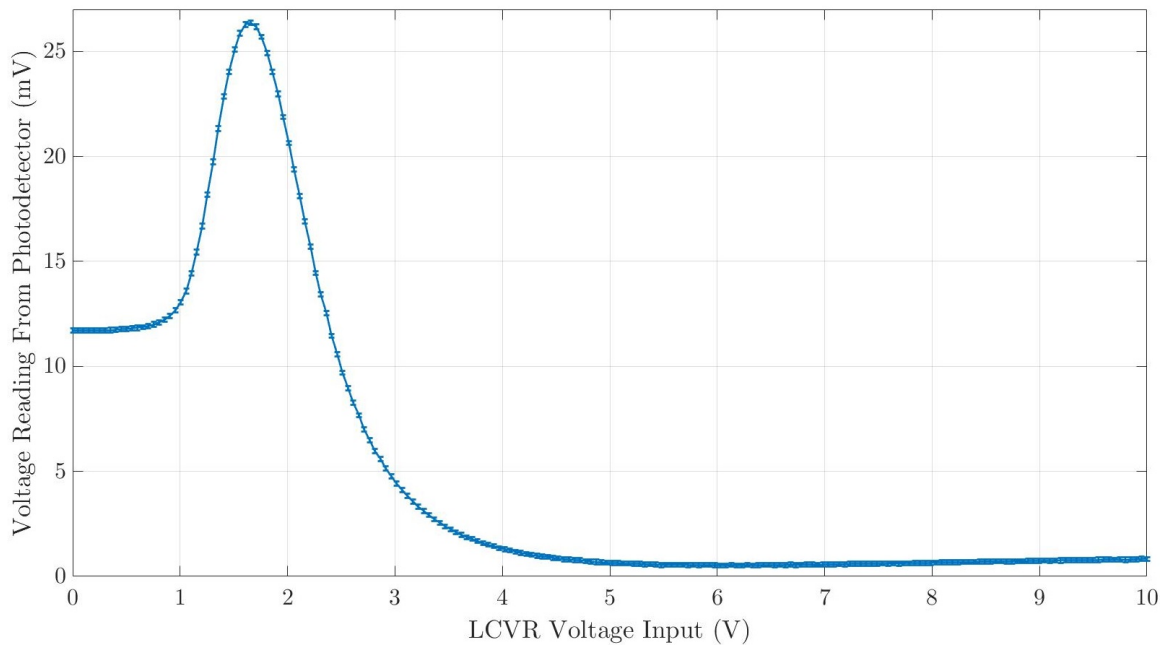


Figure A.1: Plot of mean raw voltage reading of photodetector vs LCVR voltage input for crossed polariser set-up in Figure 3.2 for the second LCVR.

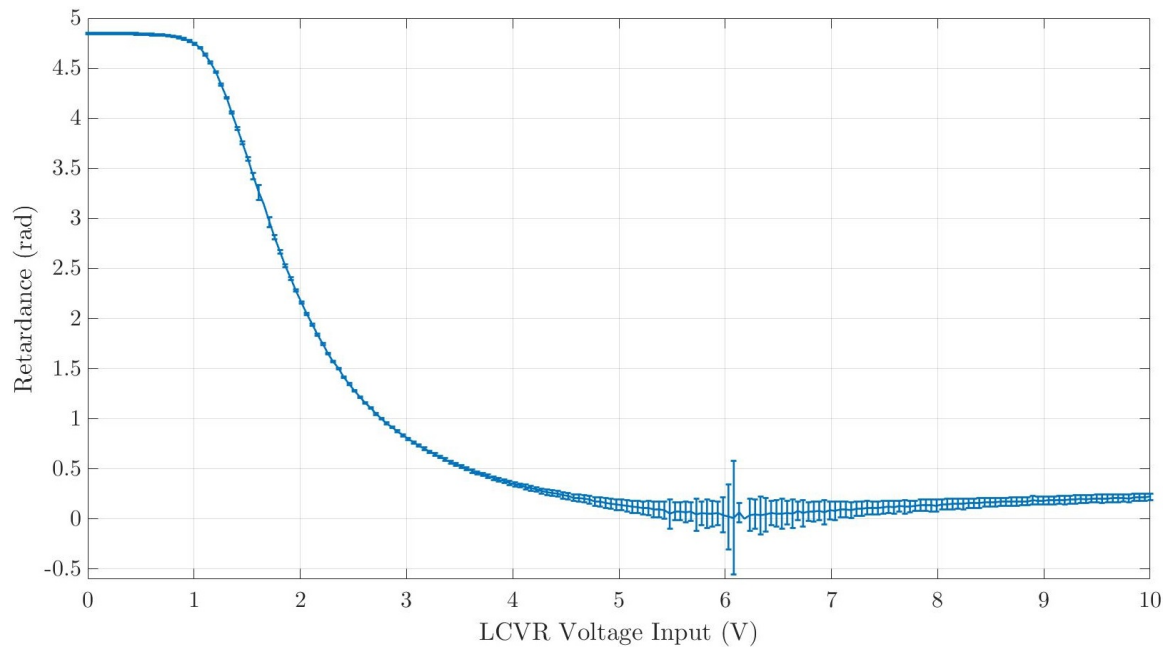


Figure A.2: Plot of LCVR retardance vs LCVR voltage input for second LCVR.

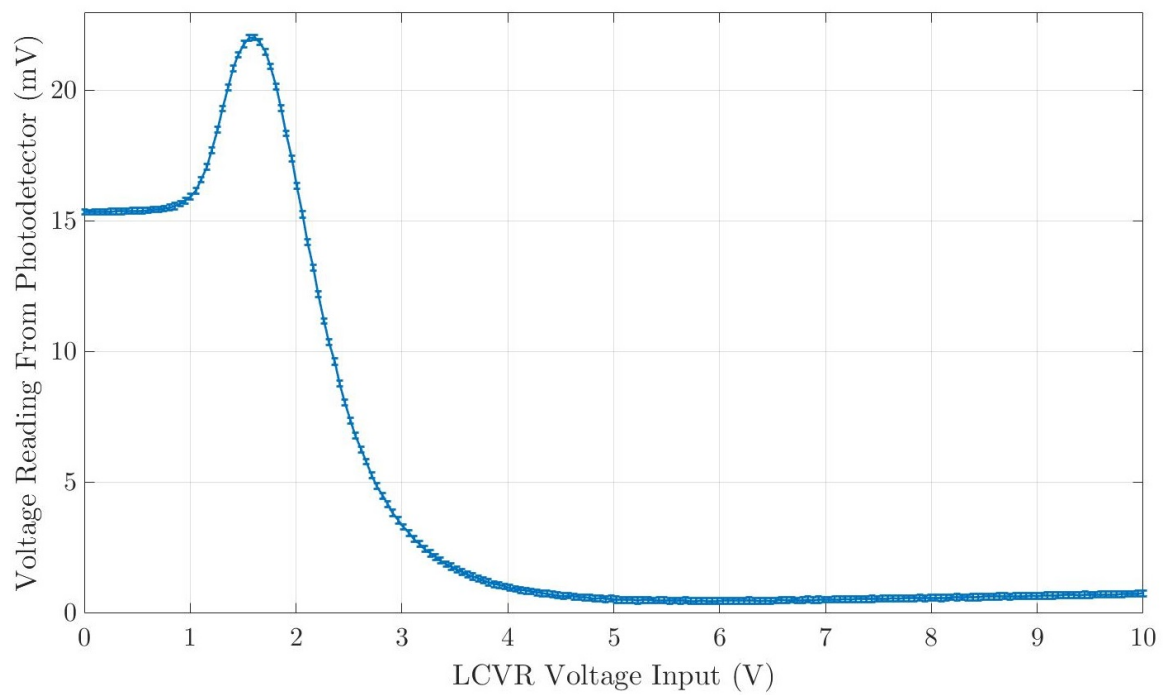


Figure A.3: Plot of mean raw voltage reading of photodetector vs LCVR voltage input for crossed polariser set-up in Figure 3.2 for the third LCVR.

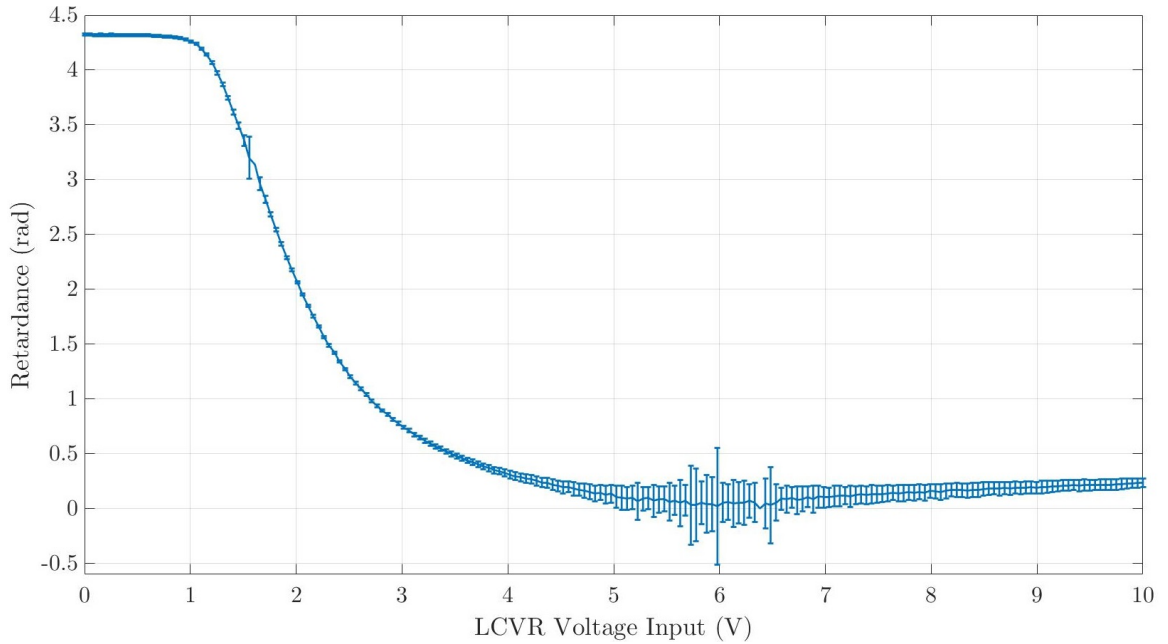


Figure A.4: Plot of LCVR retardance vs LCVR voltage input for third LCVR.

At the same time, we also tested 2 LCVRs for hysteresis effects (Note that the third and fourth LCVR is not characterised due to time constrain). Hysteresis refers to the effect in which a physical property changes differently when the cause of the change proceeds in different directions. This is vital in this project as we need to determine if the retardance characterisation of the LCVR remains consistent when the voltage input is increased and decreased. However, if there is hysteresis effects present in the LCVRs, then this effect must be accounted for in the polarisation compensation scheme.

The plots in Figure A.5 and A.6 and found that under normal testing circumstances where 50ms of buffer was given between each voltage reading from the photodetector, that there are no significant hysteresis effect in both of the LCVRs. The same retardance was obtained when the same voltage was supplied, regardless of the direction of voltage change. Thus, we regard hysteresis effect to be negligible.

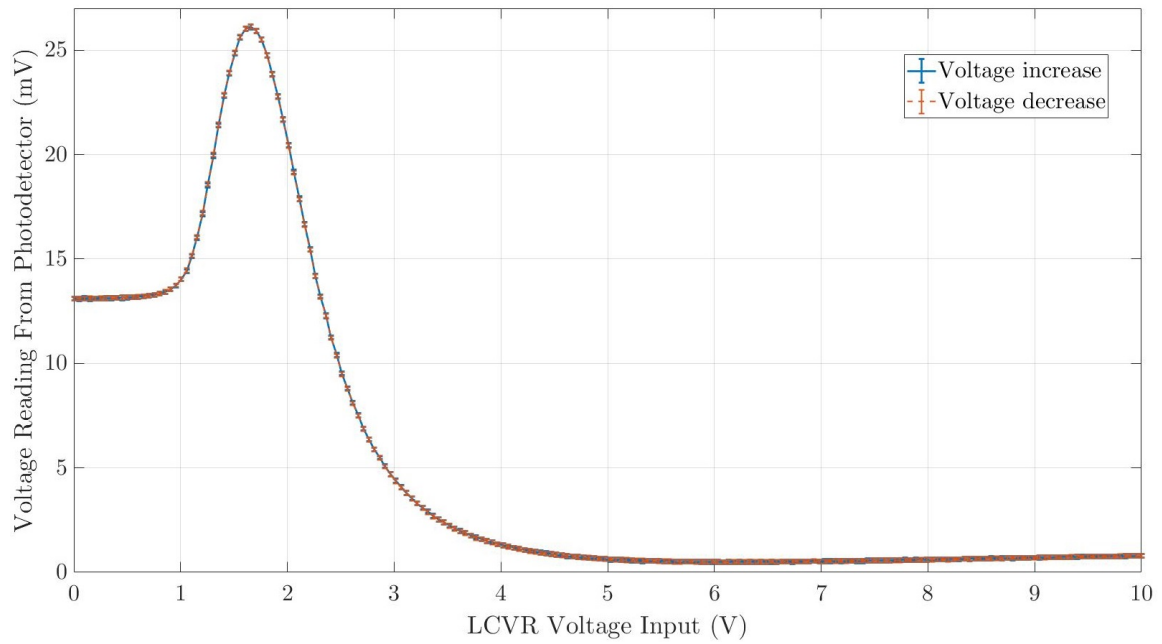


Figure A.5: Plot of mean raw voltage reading of photodetector for two separated data collection cycles. The voltage input is first increased from 0V to 10V then decreased from 10V to 0V.

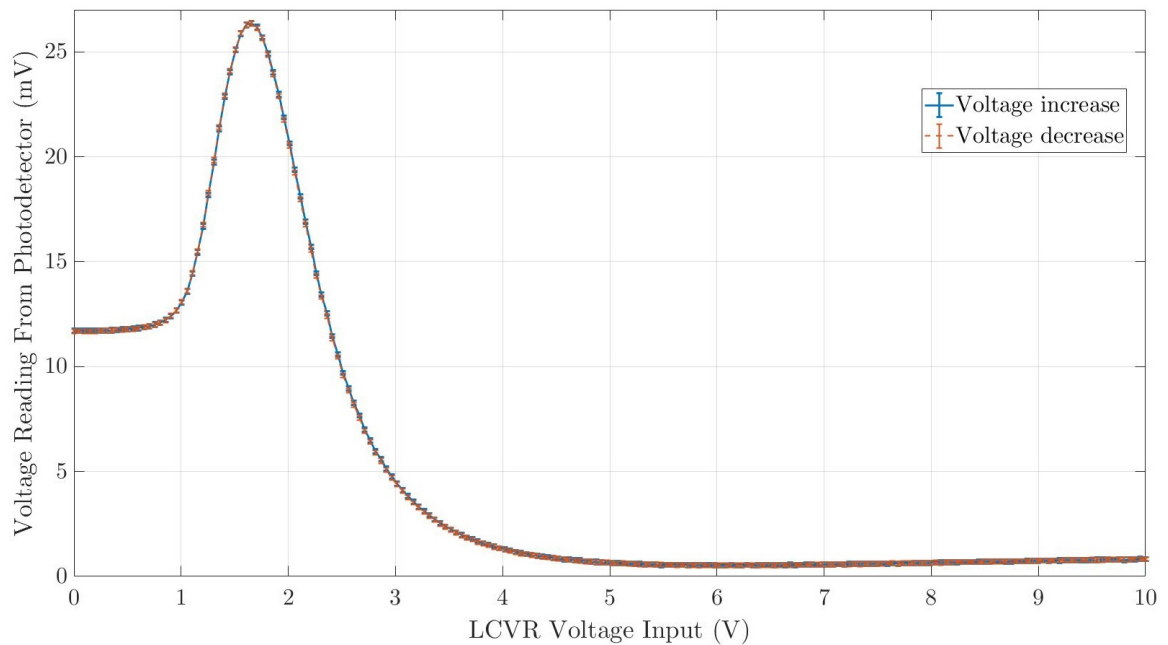


Figure A.6: Plot of mean raw voltage reading of photodetector for two separated data collection cycles. The voltage input is first increased from 0V to 10V then decreased from 10V to 0V.

Appendix B

Characterisation of Polarimeter

Further analysis of the data from the characterisation of the Polarimeter is contained in this appendix. The set-up and process is discussed in Section 3.3 and Figure 3.8 and 3.9.

The mean normalised voltage readings are shown below in Figure B.1

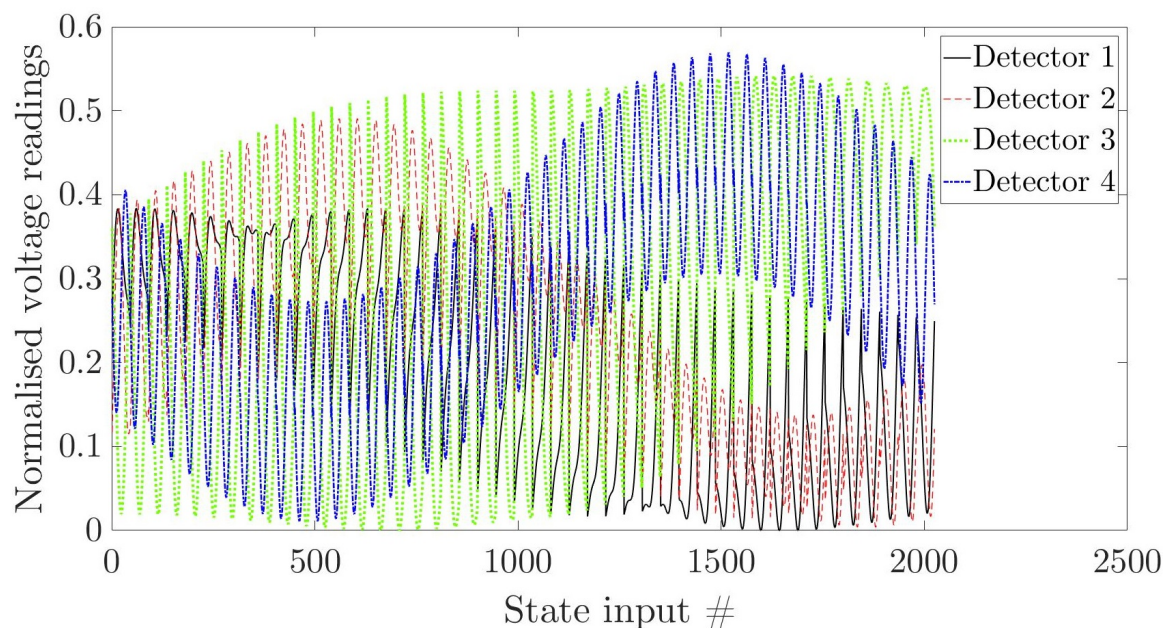


Figure B.1: Plot of mean normalised voltage readings of photodetectors in the polarimeter at each polarisation state input.

Using the mean normalised detector readings, we determine the four calibration states to be

$${}^{(1)}\vec{C} = \begin{pmatrix} 1 \\ -0.28719 \\ 0.52595 \\ 0.80056 \end{pmatrix}, {}^{(2)}\vec{C} = \begin{pmatrix} 1 \\ 0.52596 \\ 0.70261 \\ 0.47927 \end{pmatrix}, {}^{(3)}\vec{C} = \begin{pmatrix} 1 \\ -0.34855 \\ 0.02493 \\ -0.93696 \end{pmatrix}, {}^{(4)}\vec{C} = \begin{pmatrix} 1 \\ 0.07114 \\ -0.99491 \\ -0.07132 \end{pmatrix}$$

The corresponding detector readings are

$${}^{(1)}\vec{D} = \begin{pmatrix} 0.38380 \\ 0.38255 \\ 0.09920 \\ 0.13445 \end{pmatrix}, {}^{(2)}\vec{D} = \begin{pmatrix} 0.30802 \\ 0.49072 \\ 0.10625 \\ 0.09501 \end{pmatrix}, {}^{(3)}\vec{D} = \begin{pmatrix} 0.06199 \\ 0.10346 \\ 0.54185 \\ 0.29270 \end{pmatrix}, {}^{(4)}\vec{D} = \begin{pmatrix} 0.08563 \\ 0.07406 \\ 0.27085 \\ 0.56946 \end{pmatrix}$$

To compare the reconstructed states to their original polarisation inputs, we calculate the fidelity. Suppose the original Stokes vector is \vec{S} and the reconstructed Stokes vector is \vec{S}' then the fidelity, F is given by

$$F = \frac{1}{2} \vec{S}^T \vec{S}' \quad (\text{B.1})$$

The fidelity corresponds to the degree of accuracy the instrument matrix is able to reconstruct from the detector readings. For the data presented in Figure B.1 and 3.10(ii), a heat map of the fidelity is shown below

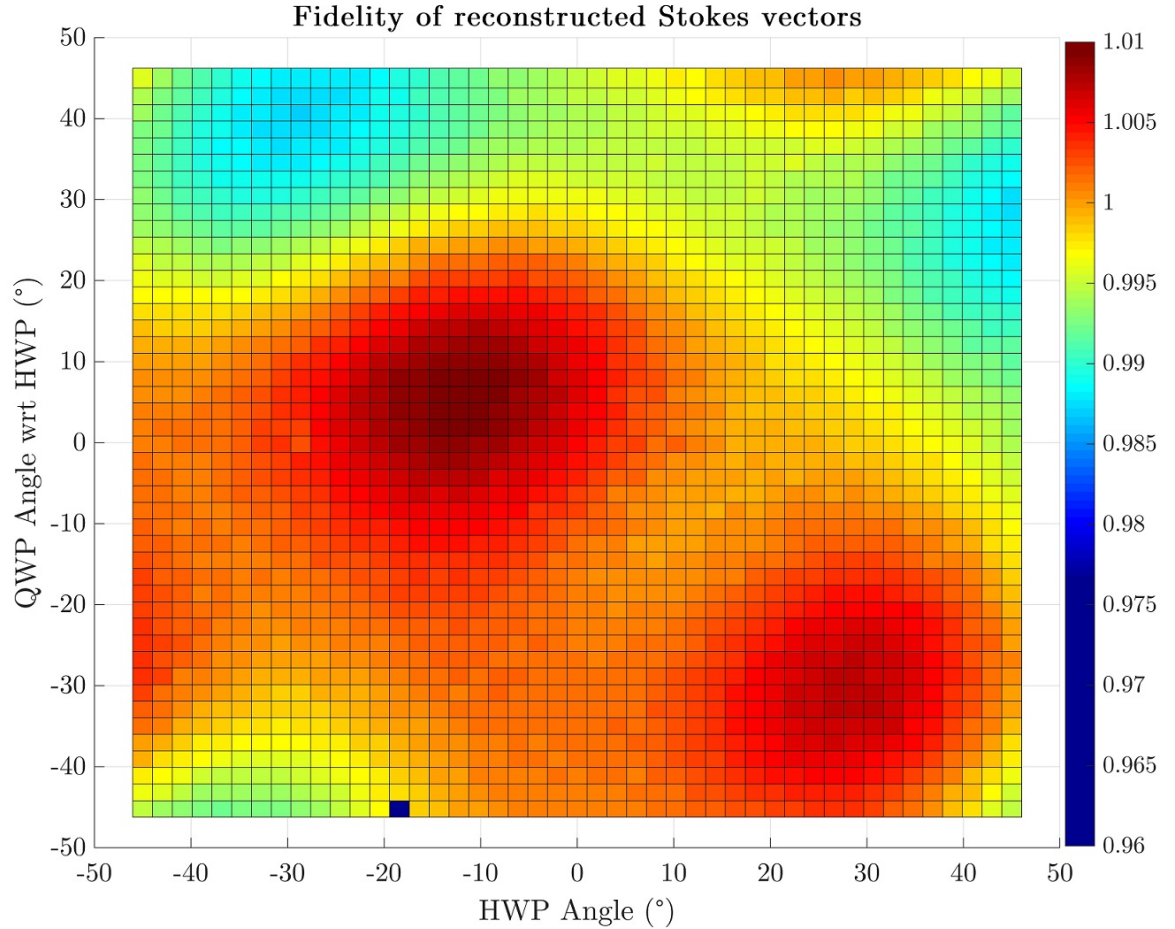


Figure B.2: Heat map of reconstructed Stokes vector shown in 3.10(ii).

Figure B.2 shows the fidelity for each reconstructed Stokes vector, in terms of the angle setting of the half-wave plate (HWP) and quarter-wave plate (QWP). The fidelity is good when it is close to 1. We see that the almost all reconstructed Stokes vectors have reasonable degree of accuracy and ranges between 0.99 to 1.01, except for one outlier near -18° for HWP and -45° for QWP of value 0.97 which still has an acceptable margin of error ($\pm 5\%$).

We also plot the degree of polarisation (without standard error bars for clarity) for completeness.

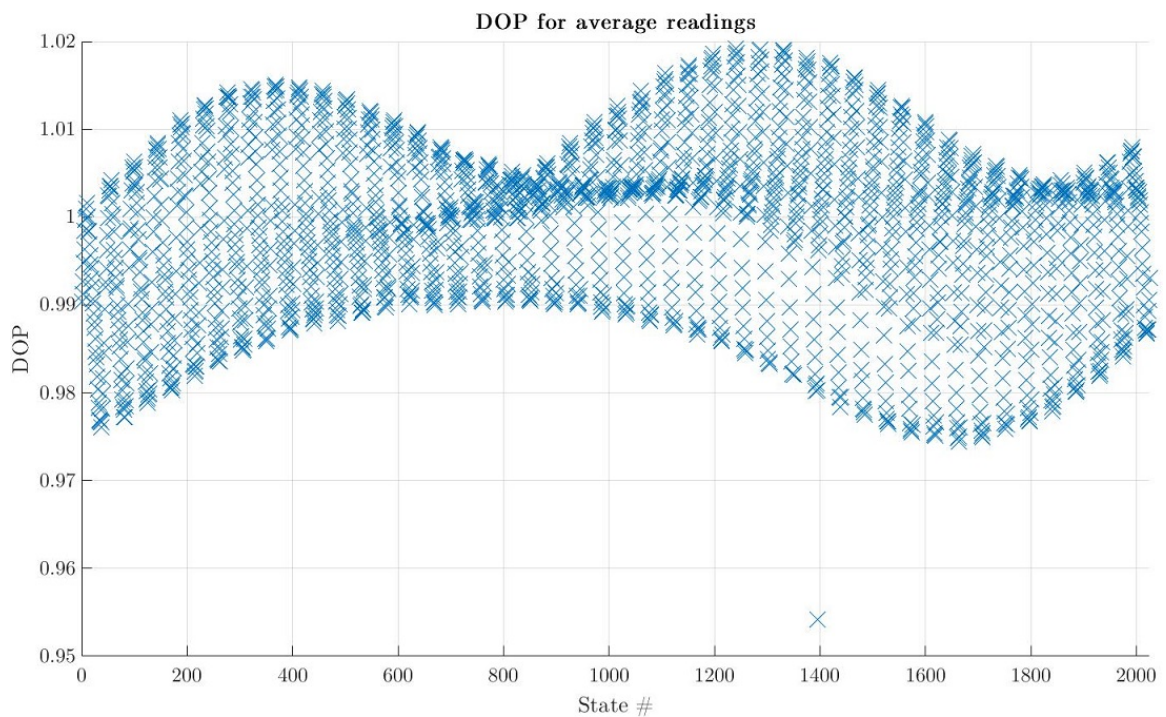


Figure B.3: Plot of Degree of Polarisation (DOP) vs state input number

Similarly, the degree of polarisation, DOP can tell us if the reconstructed states lands on the surface of the Poincaré sphere, an indicator of the degree of accuracy of the instrument matrix. We again see one outlier at about state input number 1400. However, all the reconstructed states are within the acceptable margin of error ($\pm 5\%$). Interestingly, we notice a significant number of reconstructed states have DOP larger than 1 which is likely due to the additional phase induced by the PPBS and other imperfections of the polarimeter. However, the margin of error observed is still within acceptable range for the purpose of this experiment.

Appendix C

Constant Current Mode for Laser Driver

We will be operating the laser driver in constant power output mode. However, for interest, we also investigated the constant current mode as mentioned in Section 4.1.

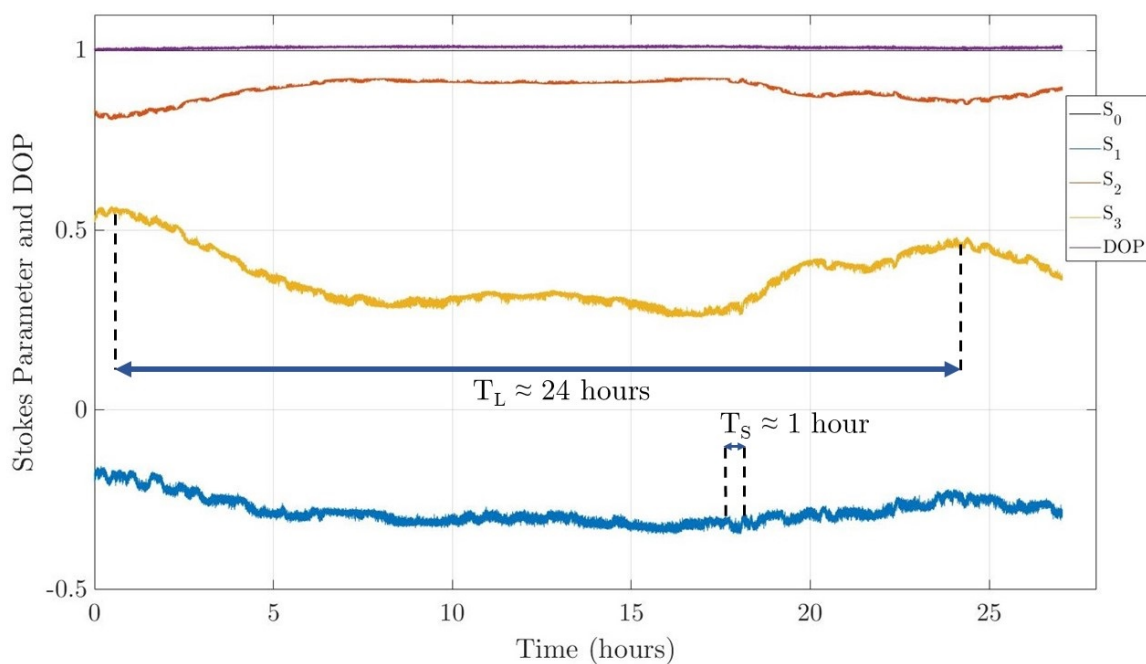
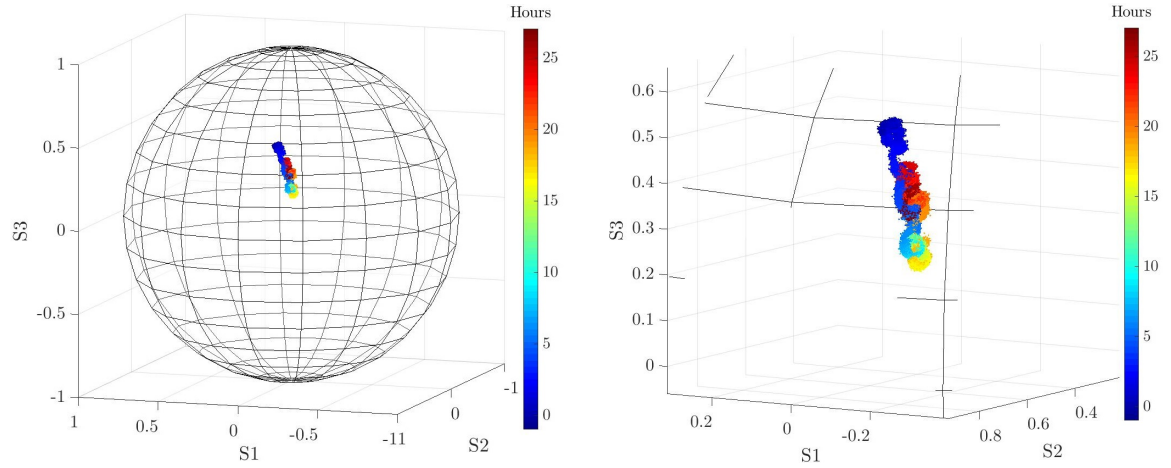


Figure C.1: Plot of Stokes parameters against time to show fluctuation in polarisation across the 1km fibre spool but at constant current mode.

From Figure C.2(i), we also see that the slower fluctuation with period labelled as T_L and the faster fluctuation T_S are similar when compared to the constant power output context shown in Figure 4.2. However, the magnitude of the slower fluctuation is now slightly higher than the constant power output context, at magnitude of ~ 0.25

as compared to ~ 0.1 in the latter case. Again, the parameter that shows the largest magnitude in fluctuation is S_3 as well.



(i) Polarisation state of the output after the 1km fibre without the LCVRs monitored over 25 hours at constant current mode.

(ii) A closer view of the polarisation drift over time from Figure C.2(i).

Figure C.2: Polarisation drift across the 1km fibre spool visualised on a Poincaré sphere at constant current mode.

This shows possible correlation between the power output of the laser diode and its polarisation output. Using constant current mode, the power output may not be consistent as the voltage input can fluctuate due to electrical noise.

Appendix D

Polarisation Drift Compensation Code

```
#!/usr/bin/env python

#####
#
# Script for Polarisation Compensation Using 4 LCVRs
#
# Author: Tan Jyh Harnng, Shi Yicheng, Poh Hou Shun
# Created: 2018.04.02
#
#####

import os
import time
import datetime
import numpy as np

import devices.polarimeter as polarimeter
import devices.rampgenerator as rampgenerator

#####

# Prepare the folder to store the data

data_folder = '/home/qitlab/programs/pol_lock/data/'
today_folder = time.strftime('%Y%m%d') + '_pol_lock'

data_path = data_folder + today_folder
if not os.path.exists(data_path):
    os.makedirs(data_path)

#####

PERIOD = 0.0005 # 2kHz frequency, specified in specs
VOLT_START = 3.5 # starts in middle of voltage range
VOLT_STEP = 0.03 # in volt
VOLT_MIN = 1.0 # in volt
```

```

VOLT_MAX = 6.0 # in volt
SLEEP_INTERVAL = 0.1 # waiting time in seconds after setting lcvr

DIST_TOL = 0.015 # trace distance tolerance

LCVR_0 = 0
LCVR_1 = 1
LCVR_2 = 2
LCVR_3 = 3

lcvr_0_volt = VOLT_START
lcvr_1_volt = VOLT_START
lcvr_2_volt = VOLT_START
lcvr_3_volt = VOLT_START

#

NO_SAMPLE = 10 # no. of sample to average

TAR_STOKES = np.array([[1], [1], [0], [0]]) # target polarisation H (s0, s1, s2, s3)

I_INV = np.matrix([[ 0.9999999999999998, 1.0000000000000001, 1.0000000000000000,
                    1.0000000000000000],
                    [5.111778511302176, 4.397609575921321, 1.007826033935272,
                    1.442549337918532],
                    [ 0.792637434396907, 1.188212671763195, 2.545790436893003,
                    1.103672083497317],
                    [ 2.988282187070310, 0.516402788626628, 0.579639255433023,
                    2.285587532078063]])

#####

DEVICE_PATH_0 = '/dev/serial/byid/usb
    Centre_for_Quantum_Technologies_Ramp_Generator_RGQO03if00'
DEVICE_PATH_1 = '/dev/serial/byid/usb
    Centre_for_Quantum_Technologies_Ramp_Generator_RGQO06if00'
DEVICE_PATH_2 = '/dev/serial/byid/usbCentre_for_Quantum_Technologies_' \
    'Tetrahedron_Polarimeter_TPRQO05if00'

#

# initialize the function generators

rg_0 = rampgenerator.RampGenerator(DEVICE_PATH_0)
rg_1 = rampgenerator.RampGenerator(DEVICE_PATH_1)

#

# initialize the polarimeter

polarimeter = polarimeter.Polarimeter(DEVICE_PATH_2)
polarimeter.set_range('3')

#####

```

```
def lcvr_all_on():
    rg_0.rectangle(0, VOLT_START, VOLT_START, PERIOD)
    rg_0.rectangle(1, VOLT_START, VOLT_START, PERIOD)
    rg_1.rectangle(0, VOLT_START, VOLT_START, PERIOD)
    rg_1.rectangle(1, VOLT_START, VOLT_START, PERIOD)

def lcvr_all_off():
    rg_0.off(0)
    rg_0.off(1)
    rg_1.off(0)
    rg_1.off(1)

# increase lcvr by 1 voltage step
def lcvr_incr(channel):
    global lcvr_0_volt, lcvr_1_volt, lcvr_2_volt, lcvr_3_volt
    global VOLT_STEP, VOLT_MAX, PERIOD, SLEEP_INTERVAL
    if channel == 0:
        if lcvr_0_volt + VOLT_STEP < VOLT_MAX:
            lcvr_0_volt = lcvr_0_volt + VOLT_STEP
            rg_0.rectangle(0, lcvr_0_volt, lcvr_0_volt, PERIOD)
        else:
            print "lcvr 0 over VOLT_MAX!"
            lcvr_0_volt = VOLT_START # reset voltage is over range
    elif channel == 1:
        if lcvr_1_volt + VOLT_STEP < VOLT_MAX:
            lcvr_1_volt = lcvr_1_volt + VOLT_STEP
            rg_0.rectangle(1, lcvr_1_volt, lcvr_1_volt, PERIOD)
        else:
            print "lcvr 1 over VOLT_MAX!"
            lcvr_1_volt = VOLT_START
    elif channel == 2:
        if lcvr_2_volt + VOLT_STEP < VOLT_MAX:
            lcvr_2_volt = lcvr_2_volt + VOLT_STEP
            rg_1.rectangle(0, lcvr_2_volt, lcvr_2_volt, PERIOD)
        else:
            print "lcvr 2 over VOLT_MAX"
            lcvr_2_volt = VOLT_START
    elif channel == 3:
        if lcvr_3_volt + VOLT_STEP < VOLT_MAX:
            lcvr_3_volt = lcvr_3_volt + VOLT_STEP
            rg_1.rectangle(1, lcvr_3_volt, lcvr_3_volt, PERIOD)
        else:
            print "lcvr 3 over VOLT_MAX"
            lcvr_3_volt = VOLT_START
    time.sleep(SLEEP_INTERVAL)

# increase lcvr by 1 voltage step
def lcvr_decr(channel):
    global lcvr_0_volt, lcvr_1_volt, lcvr_2_volt, lcvr_3_volt
    global VOLT_STEP, VOLT_MIN, PERIOD, SLEEP_INTERVAL
    if channel == 0:
        if lcvr_0_volt - VOLT_STEP > VOLT_MIN:
```

```

        lcvr_0_volt = lcvr_0_volt + VOLT_STEP
        rg_0.rectangle(0, lcvr_0_volt, lcvr_0_volt, PERIOD)
    else:
        print "lcvr 0 under VOLT_MIN!"
        lcvr_0_volt = VOLT_START # reset voltage is over range
elif channel == 1:
    if lcvr_1_volt + VOLT_STEP > VOLT_MIN:
        lcvr_1_volt = lcvr_1_volt + VOLT_STEP
        rg_0.rectangle(1, lcvr_1_volt, lcvr_1_volt, PERIOD)
    else:
        print "lcvr 1 under VOLT_MIN!"
        lcvr_1_volt = VOLT_START
elif channel == 2:
    if lcvr_2_volt + VOLT_STEP > VOLT_MIN:
        lcvr_2_volt = lcvr_2_volt + VOLT_STEP
        rg_1.rectangle(0, lcvr_2_volt, lcvr_2_volt, PERIOD)
    else:
        print "lcvr 2 under VOLT_MIN!"
        lcvr_2_volt = VOLT_START
elif channel == 3:
    if lcvr_3_volt + VOLT_STEP > VOLT_MIN:
        lcvr_3_volt = lcvr_3_volt + VOLT_STEP
        rg_1.rectangle(1, lcvr_3_volt, lcvr_3_volt, PERIOD)
    else:
        print "lcvr 3 under VOLT_MIN!"
        lcvr_3_volt = VOLT_START
time.sleep(SLEEP_INTERVAL)

#

def dist():
    global I_INV, TAR_STOKES, NO_SAMPLE
    readings = np.array([0, 0, 0, 0])
    for i in range(NO_SAMPLE):
        pol_int_vec_1, pol_int_vec_2, pol_int_vec_3, pol_int_vec_4 = polarimeter.volt()
        readings = readings + np.array([pol_int_vec_1, pol_int_vec_2, pol_int_vec_3,
            pol_int_vec_4])
    stokes = np.array(I_INV*np.transpose(np.matrix(readings/sum(readings), dtype=float)))
    distance = np.linalg.norm(stokes - TAR_STOKES)
    curr_time = datetime.datetime.now()
    print float(stokes[0]), float(stokes[1]), float(stokes[2]), float(stokes[3]), distance,
        lcvr_0_volt, lcvr_1_volt, lcvr_2_volt, lcvr_3_volt, curr_time
    f.write('{0:.3e}\t{1:.3e}\t{2:.3e}\t{3:.3e}\t{4:.3e}\t{5:.3e}\t{6:.3e}\t{7:.3e}\t{8:.3e}\t{9}\n'.format(float(stokes[0]), float(stokes[1]), float(stokes[2]), float(stokes[3]),
        distance, lcvr_0_volt, lcvr_1_volt, lcvr_2_volt, lcvr_3_volt, curr_time))
    return distance

#

def descent():
    old_dist = dist()
    for i in range(0,4):
        lcvr_incr(i) # try voltage step increase
        if dist() > old_dist:

```

```
    levr_decr(i) # cancel last voltage step increase
    levr_decr(i) # try voltage step decrease
    if dist() > old_dist: # already at minimum, restore to starting voltage
        levr_incr(i)

#####

levr_all_on()

#####

# locking

output_file = time.strftime("%Y%m%d_%H%M_pol_lock.dat")
output_file = data_path + '/' + output_file

with open(output_file, 'w') as f:

    while 1:
        if dist() > DIST_TOL:
            descent()

#####
```

Bibliography

- [1] Geek3. Poincare sphere. https://commons.wikimedia.org/wiki/File:Poincare-sphere_arrows.svg, 2014.
- [2] Meadowlark Optics. *Meadowlark Optics Catalog*, 2008.
- [3] Michael A. Nielsen and Isaac L. Chuang. *Quantum Computation and Quantum Information*. Cambridge University Press.
- [4] Hewlett-packard development company, quantum information processing. <http://www.hp1.hp.com/research/qip/>, 2009.
- [5] Ibm t.j. watson research center, quantum cryptography. https://researcher.watson.ibm.com/researcher/view_page.php?id=7242, 1984.
- [6] Toshiba research europe ltd., cambridge research laboratory, quantum information group, quantum key server. <https://web.archive.org/web/20070430232220/http://www.toshiba-europe.com/research/crl/qig/quantumkeyserver.html>, 2007.
- [7] Akshata Shenoy-Hejamadi, Anirban Pathak, and Srikanth Radhakrishna. Quantum cryptography: Key distribution and beyond. *Quanta*, 6(1):1–47, 2017.
- [8] Mart Haitjema. A survey of the prominent quantum key distribution protocols. <http://www.cse.wustl.edu/~jain/cse571-07/ftp/quantum/>.
- [9] Charles H. Bennett, Gilles Brassard, and N. David Mermin. Quantum cryptography without bell’s theorem. *Phys. Rev. Lett.*, 68:557–559, Feb 1992.
- [10] D. Goldstein and B. Thompson. *Polarized Light, Revised and Expanded*. Boca Raton: CRC Press., 2003.
- [11] Alexander L., K.P Soh, Antia Lamas-Linares, and Christian Kurtsiefer. An optimal photon counting polarimeter.

- [12] G B Xavier, N Walenta, and et al. Experimental polarization encoded quantum key distribution over optical fibres with real-time continuous birefringence compensation. 11.
- [13] Z. L. Yuan and A. J. Shields. Continuous operation of a one-way quantum key distribution system over installed telecom fibre. 13.
- [14] A. Muller, T. Herzog, B. Huttner, W. Tittel, H. Zbinden, and N. Gisin. “plug and play” systems for quantum cryptography. *Applied Physics Letters*, 70(7):793–795, 1997.
- [15] R. Paschotta. Polarization-maintaining fibers. https://www.rp-photonics.com/polarization_maintaining_fibers.html.
- [16] E. Hecht. *Optics*. Pearson, 2014.
- [17] R. M. A. Azzam, I. M. Elminyawi, and A. M. El-Saba. General analysis and optimization of the four-detector photopolarimeter. *J. Opt. Soc. Am. A*, 5(5):681–689, May 1988.
- [18] Jaroslav Řeháček, Berthold-Georg Englert, and Dagomir Kaszlikowski. Minimal qubit tomography. *Phys. Rev. A*, 70:052321, Nov 2004.
- [19] D. S. Sabatke, M. R. Descour, E. L. Dereniak, W. C. Sweatt, S. A. Kemme, and G. S. Phipps. Optimization of retardance for a complete stokes polarimeter. *Opt. Lett.*, 25(11):802–804, Jun 2000.
- [20] Dwight C. Look Amrit Ambirajan. Optimum angles for a polarimeter: part ii. *Optical Engineering*, 34:34 – 34 – 3, 1995.
- [21] Info communications Media Development Authority. Optical fibre deployment. *Next Generation National Broadband Network (NGNBN)*, October 2016.
- [22] International Telecommunication Union. Characteristics of a single-mode optical fibre and cable. *Telecommunication Standardization Sector of ITU*, November 2016.
- [23] Thorlabs Inc. *LP1310-SAD2 Specification Sheet*, July 2015.
- [24] Jonathan Strickland. What is a gimbal – and what does it have to do with nasa? <https://science.howstuffworks.com/gimbal.htm>.

- [25] Corning Inc. *Corning SMF-28e+ Optical Fibre*, July 2014.
- [26] Thorlabs Inc. *ITC4000 Series Operation Manual*, October 2017.
- [27] J.M.Mendel. Gradient, error-correction identification algorithms. 11:23–42.